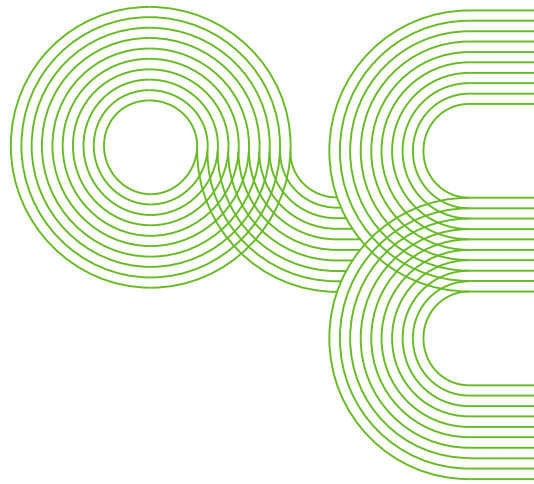


Universidade de Vigo

Memoria de traballo de fin de grao

Escola de Enxeñaría Aeronáutica e do Espazo



Autor: César Crego Loureiro

Titulación: Ingeniería Aeroespacial

Título do traballo: **Numerical modelling of wave energy converters**

Titor: Alejandro Jacobo Cabrera Crespo

Co-titor: José Manuel Domínguez Alonso

Data: 16 de xuño de 2021

*... Un vello, arrimado nun pau de sanguinho,
o monte atravesa de cara ó piñar.
Vai canso; unha pedra topou no camino
e nela sentouse para folgos tomar...*

Manuel Curros Enríquez

Agradecimientos

Quiero agradecer al grupo *EPhysLab* por la oportunidad de realizar con ellos este trabajo y sobre todo por acogerme como uno más desde el día cero. Iván, Ángel, Salvatore o Bonaventura, gracias por vuestra compañía durante estos meses. A Jose por su contribución en este trabajo, también gracias.

Gracias en especial a Álex, quien me ha ayudado y guiado durante toda esta experiencia, haciendo realmente entretenido y sencillo el trabajar en este proyecto. Es una suerte trabajar así.

Este trabajo pone fin a una etapa más de crecimiento, en la que he conocido muchos compañeros y amigos. A todos ellos, gracias por coexistir y crecer conmigo.

Por último, gracias a mi familia por ayudarme y formar parte en todas las etapas que voy superando. Os siento a todos.

Resumen

La energía undimotriz se plantea como una alternativa potencialmente viable a los combustibles fósiles en un futuro cercano y con cero emisiones de gases de efecto invernadero. Sin embargo, aún no hay unanimidad sobre cuál es la tecnología más eficiente para aprovechar la energía de las olas y así convertir a este tipo de energía renovable en un recurso rentable.

Este trabajo fin de grado analiza las posibilidades del modelado numérico para ayudar a diseñar dispositivos de captación de energía de olas. El estudio se centra en el dispositivo llamado FOSWEC que ha sido diseñado por los laboratorios SANDIA, en EEUU. Este dispositivo es realmente complejo, puesto que incluye diferentes partes flotantes, amarres anclados al fondo y la producción de energía se basa en los movimientos oscilatorios de dos aletas gracias a unos engranajes con un sistema de toma de fuerza (*Power Take Off* en inglés). La complejidad del FOSWEC, convierte en un verdadero reto la ejecución de una simulación fiable utilizando una única herramienta numérica. El grupo *EPhysLab* de la *Universidad de Vigo* ha desarrollado un software libre llamado *DualSPHysics* basado en el método libre de malla SPH, y que será el utilizado en este estudio.

Después de un periodo inicial de aprendizaje en el manejo del software *DualSPHysics*, se realiza una validación comparando las simulaciones con datos experimentales proporcionados por SANDIA. De esta manera demostramos que el software es capaz de reproducir la respuesta hidrodinámica de este complejo dispositivo bajo la acción de un tren de olas regulares.

Una vez validada la herramienta, se realiza un estudio de eficiencia del FOSWEC, demostrando que gracias a la herramienta se pueden obtener configuraciones óptimas del dispositivo FOSWEC para diferentes condiciones de oleaje regular, y en tiempos significativamente menores al proceso de fabricación y ensayo experimental.

Cabe destacar que no existe otro modelo computacional similar que incluya todas las potencialidades de *DualSPHysics* y que esté disponible para su descarga gratuita por toda la comunidad científica. Este tipo de modelos son una gran alternativa para ayudar en el diseño de dispositivos captadores de energía de las olas y este trabajo contribuye a mostrar sus capacidades.

Index

1. Introduction	8
2. Objectives	10
3. Wave energy	11
3.1 Climate change and importance of renewable energies	11
3.2 Wave energy and energy potential	14
3.3 Wave Energy Converters	15
3.4 FOSWEC device	16
4. Numerical modelling	18
4.1 Smoothed Particle Hydrodynamics method	19
4.2 DualSPHysics code	23
4.3 Discretization with particles	25
4.4 Coupling with Project Chrono and with MoorDyn	26
5. Validation	28
5.1 Experimental configuration	28
5.2 Numerical setup	30
5.3 Wave generation, propagation and absorption	34
5.4 Motions of the hull	37
5.5 Mooring tensions	39
5.6 Motions of the flaps	42
6. Efficiency analysis	43
7. Conclusions and future work	48
References	50
Appendix	53

Index of figures

Figure 3.1. Growth of greenhouse effect gases. Source: IPCC 2007.	11
Figure 3.2. Annual wave energy distribution. Source: IDAE (2011).	14
Figure 3.3. WEC types according to the capture principle.	16
Figure 3.4. FOSWEC device. Source: https://youtu.be/OUxbaEC2K6Y	17
Figure 4.1. Representation of the kernel function.	20
Figure 4.2. Institutions developing DualSPHysics.	23
Figure 4.3. DualSPHysics package: Pre-processing, solver & post-processing tools.	24
Figure 4.4. Object discretization using different resolutions.	25
Figure 4.5. Flow chart of the coupling of DualSPHysics with Project Chrono and with MoorDyn.	27
Figure 5.1. Dimensions of the wave basin and location of FOSWEC and the wave gauges during the experimental campaign.	29
Figure 5.2. FOSWEC dimensions.	30
Figure 5.3. Numerical wave tank for R5C (top and lateral view).	31
Figure 5.4. Piston wavemaker and damping zone in the numerical tank designed for wave generation and propagation.	34
Figure 5.5. Different instants of the wave propagation during a period ($\Delta p=0.02$ m).	35
Figure 5.6. Time series of experimental and numerical free-surface elevation.	36
Figure 5.7. Different instants of the interaction between regular waves and FOSWEC during a period ($\Delta p=0.02$ m).	37
Figure 5.8. Time series of experimental and numerical heave, surge and pitch.	38
Figure 5.9. Time series of experimental and numerical mooring tensions.	39
Figure 5.10. Particle discretization of the FOSWEC device for different resolutions. ...	40
Figure 5.11. Time series of experimental and numerical mooring tensions for different resolutions obtained in the still water test.	41
Figure 5.12. Time series of experimental and numerical angles of bow and aft flaps. ...	42
Figure 6.1. Time series of the angular velocity of the flaps for different resolutions. ...	44
Figure 6.2. Wave power and power absorbed by FOSWEC for different wave periods.	46
Figure 6.3. Efficiency of FOSWEC as function of wave period and for different PTO systems.	47

Index of tables

Table 3.1. Annual production potential of marine energies. Source: IDAE (2011).....	13
Table 5.1. Different conditions of the regular waves.	28
Table 5.2. Wave conditions of experimental setup R5C.	31
Table 5.3. Features of the floating parts of FOSWEC.	32
Table 5.4. Stiffness and damping coefficients of the PTO system.....	32
Table 5.5. Information about the four mooring lines.	33
Table 5.6. Resolution, number of particles and runtime.	33
Table 6.1. Power and efficiency results of R5C.	45
Table 6.2. Different wave conditions used in the efficiency study.	45
Table 6.3. Different PTO configurations used in the efficiency study.....	45

1. Introduction

According to Falnes (2007) the world power consumption nowadays is the order of 10 TW (10^{13} W). It has been estimated that seas and oceans could be capable to supply this all power if marine energies get to be efficient. At present, there are thousands of devices, already patented, which aim to capture kinetic energy carried by waves on its movement (wave energy). However, a concrete type of technology that can manifest a clear higher efficiency above the other has not been found yet. The technological growth of this energy is a major challenge since it is an energy with huge potential and at an early development phase.

The devices that can harness the wave energy are called *Wave Energy Converters* (WEC) and it is imperative to characterise properly their behaviour to contribute to their development. One of the most challenging aspects is to describe their operation for several wave conditions, paying special attention to the device energy efficiency and to its survivability or endurance when interacting with very energetic waves.

Despite the benefits that marine energies do have (non-pollute, great energy potential, etc.) the pursuit of a specific WEC, which may remain above the rest in efficiency it is not an easy task. The production implies elevated costs not only in the phase of creating the WEC, but also in the investment to build the facilities where the device will be tested. Due to this, and thanks to the massive growth of computers for calculation, tools based on *Computational Fluid Dynamics* (CFD) are performing an essential role for the research and evolution of these energy converters. CFD tools reduce immensely the costs and provide very accurate results.

Some of the most popular CFD methods are the mesh-based ones, which often use *Finite Volume Element* methods to discretize the domain. However, these methods have difficulties when discretizing complex moving geometries such as WECs and cases with large deformations of the free surfaces such as ocean waves interacting with the floating offshore devices. This is why a meshfree method called *Smoothed Particle Hydrodynamics* (SPH) will be used for our study. All the results will be obtained from the use of the *DualSPHysics* software, which has been developed, among other institutions, by the research group *EPhysLab* at *University of Vigo*.

Due to the previous success of the *DualSPHysics* software applied for the simulation of WECs (Crespo et al., 2017, Roperó-Giralda et al., 2020, Quartier et al., 2021), several companies and institutions have contacted the group looking for new collaborations. As an example, *EPhysLab* has been collaborating with SANDIA National Laboratories for more than two years. SANDIA is a major research centre working on the development of WECs. They have enormous facilities where they perform physical tests with devices designed by them. As a result of this collaboration, it should be highlighted the journal paper by Roperó-Giralda et al. (2021), in which a point-absorber developed by SANDIA was successfully modelled with SPH.

SANDIA has recently developed a new energy converter named *Floating Oscillating Wave Energy Converter* (FOSWEC) (Coe et al., 2020). The FOSWEC is a complex design, which will be very challenging to be simulated with any CFD tool. The device includes a floating body that it is attached to the bottom of a basin with mooring lines and two flaps whose PTO system is based on the angular motion along the hinges that connect the flaps to the main body.

The main objective of this study is to prove that the *DualSPHysics* software is capable to simulate such a complex wave energy converter like FOSWEC. Some physical test will be reproduced with the numerical tool comparing the results with the ones obtained by SANDIA in their facilities. Next an efficiency study will be carried out with the validated tool, considering the action of different wave conditions and different PTO systems of FOSWEC.

The document is organised as follows: chapter 2 includes the main and more specific objectives of this end of degree project; chapter 3 addresses the wave energy resource and the FOSWEC technology; chapter 4 describes the SPH methodology and the *DualSPHysics* software; chapter 5 presents the validation for one of the physical tests carried out in SANDIA; chapter 6 includes the efficiency study; and chapter 7 discusses the main conclusions of this work and the lines for future work.

2. Objectives

The main purpose of this work is being able to prove the capability of the *DualSPHysics* software to study the hydrodynamic response of the FOSWEC device under train of regular waves, and taking advantage of this capability to help on the development of the energy converter.

In order to reach the main objective, it will be necessary to acquire several skills and achieve specific objectives such as the ones listed below:

- Discovering a CFD software different from mesh-based ones learned throughout the bachelor, which are suitable for the majority of application fields in aeronautics. In this work a novel meshfree particle methodology will be used, since it presents several advantages when dealing with wave-WEC interactions.
- Learning about the basis of the *Smoothed Particle Hydrodynamics* (SPH) method, that is a fully Lagrangian particle method that solves de *Navier-Stokes* equations.
- Acquiring the skills to create simulation cases with the *DualSPHysics* software, to run simulations on the CPU and on the GPU (matter of interest since GPU simulations will reduce computational time significantly), to analyse results thanks to the post-processing tools and to create images and videos to display the results.
- Performing a validation where SPH results are compared with experimental data. In this validation the main features of the physical test will be reproduced in the numerical simulation, and the differences between numerical and experimental system will be discussed.
- Applying the validated tool to carry out an efficiency study for different regular wave conditions and FOSWEC configurations, defining the efficiency of the device as the ratio between the energy absorbed and the energy available in the wave, aiming to find a configuration that maximizes the energy absorbed by the device.

3. Wave energy

Oceans are considered to be the best collector for solar energy and the biggest system for energy storage. This huge energy potential can be turned into electricity through several technologies and satisfy energetic needs in nowadays society. The source of energy stored in oceans may be manifested in different ways which will be mentioned further in this document. If all these technologies were used efficiently, we would be gathering enormous amounts of electrical energy.

3.1 Climate change and importance of renewable energies

The influence of the human being on climate change is evident as recent emissions of greenhouse effect gases are the highest in history (IPCC, 2007). Modern climate changes have had a significant impact in human and environmental systems.

Global warming is doubtless, since 1950s we have experienced several changes in our environment with no precedents in history. Atmosphere and oceans have heated up, the amounts of snow and ice surface (the poles) are decreasing and sea level has increased. According to this, the period between 1983-2012 is likely to be the hottest 30-year period for the north hemisphere in the last 1400 years.

As a result of demographic and economic growth all abroad the globe, *Greenhouse effect* gases concentration have increased since preindustrial period, reaching their historical peak. The consequences of these levels of CO₂, CH₄, and N₂O have been clearly perceived in global warming and it is very probable to be the main cause for the rising temperatures in the late 20th century. In Figure 3.1 the significant growth of greenhouse effect gases since 1850s until present can be observed.

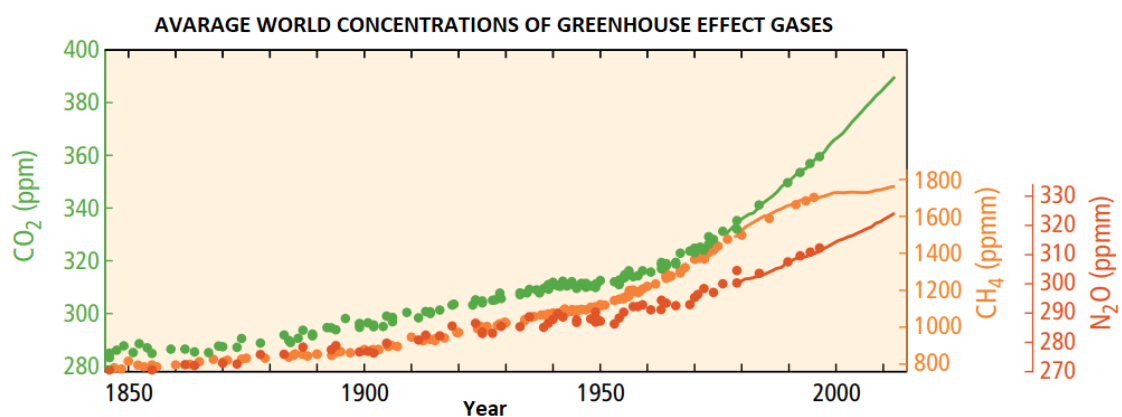


Figure 3.1. Growth of greenhouse effect gases. Source: IPCC 2007.

Obtaining energy from fossil fuels is the major cause of carbon emissions in the atmosphere, and consequently, principal responsible for global warming. In addition to this, fossil fuels are willing to finish, as we are consuming them faster than they can be generated. Nevertheless, the need of energy due to economic and social development is still growing. Hence, we must find new alternative paths for obtaining energy which may satisfy our needs. Sustainable energies are an alternative that each day becomes more feasible. Renewable (or sustainable) energies are obtained out of natural sources or processed considered to be constantly replenished. There is a huge variety of this kind of energies among of them we can highlight the following:

- *Solar energy*: It gets power out of the sun. The main technologies used are photovoltaic solar energy, which uses light of the sun to obtain power; and thermal solar energy, which uses the heat fired by the sun.
- *Wind energy*: It uses wind kinetic energy to move the blades of a propeller and to produce electrical energy out of this movement. These propellers are called aerogenerators and they can be placed on the ground or on the sea (*offshore*).
- *Biomass Energy*: It is obtained out of organic substances. However, it necessary its combustion to get the energy (either organic matter, biodiesel or bioethanol) which produces CO₂ and other greenhouse effect gases.
- *Geothermal energy*: It is the thermal generated and stored in the inner Earth.
- *Hydraulic energy*: It transforms kinetic and potential energy from rivers, waterfalls, etc. It can be referred as “hydroelectric” since it is mainly converted to electricity.
- *Hydrogen energy*: It is an alternative source of energy which uses a technology similar to batteries, where hydrogen is the fuel. Hydrogen is very abundant, efficient and a non-pollute fuel. It is, though, a technology still in growth.
- *Marine energy*: Seas and oceans are rich in several types of energy such as potential, kinetic, chemical or thermal. Marine energies can exploit any of those to harvest energy.

According to the *IDEA* (2011), Spain should be consuming 20.8%, of its overall final consumption, out of renewable energies. Although our country has not reached the objectives defined for 2020, the sector has experienced the highest growth rate from the last 8 years. Nevertheless, Spain should keep increasing its consumption out of renewable energies. Europe is aiming to reduce in 2030 the greenhouse gasses emission by at least 40% comparing to data in 1990, and to be climate neutral by 2050 (European Commission, 2020). To reach this objective, Europe should change its energy policy, so does Spain. One of the paths that Europe wants to follow is to upscale and diversify the implementation of renewable systems. This fact should accelerate the growth of upcoming energies. Particularly, EU is seriously confident in the future development of marine energies, stated that offshore renewable energies have the potential to supply 10% (100 GW) of Europe’s electricity consumption by 2050 (ETIPOCEAN 2020).

Going in depth, in this study we want to highlight the importance of marine science on this energetic growth. According to International Energy Agency, the estimated world potential of electrical energy coming out of marine energy is 120 000 TWh per year. Here by the different marine energies are listed:

- Tidal Energy: Obtains energy from kinetic power of the tides.
- Wave Energy: Obtains energy from kinetic power of the waves.
- Ocean Thermal Energy: Obtains energy from thermal power of the oceans.
- Salinity Gradient Energy: Obtains energy from chemical reactions in oceans.
- Currents Energy: Obtains energy from kinetic power of sea currents.

This energy potential can be broken down into all the different technologies which subtract energy from seas and oceans. We can see the contribution of each technology in the Table 3.1.

Table 3.1. Annual production potential of marine energies. Source: IDAE (2011).

Energy	Production potential [TWh/year]
Tidal Power	300
<i>Wave Power</i>	<i>8,000-80,000</i>
Ocean Thermal	10,000
Salinity Gradient	2,000
Currents	800

3.2 Wave energy and energy potential

As mentioned above, wave energy is the energy obtained out of the oscillatory movement of the water surface of seas and oceans. This energy comes somehow from solar energy, as sun heats Earth surface, which produces wind, which finally produces the waves. Waves have the ability of traveling long distance and barely lose energy. This energy is a constant and predictable energy, with a less damaging impact on environment than other technologies.

The areas with highest wave energy potential are placed at Atlantic and Pacific oceans, between 40° and 65° latitude, with a potential among 50-100 KW per meter of wave. Figure 3.2 shows annual distribution of wave energy potential over the globe. It can be observed that the highest potential is placed at the Indic Ocean, followed by the areas mentioned before at Atlantic and Pacific oceans.

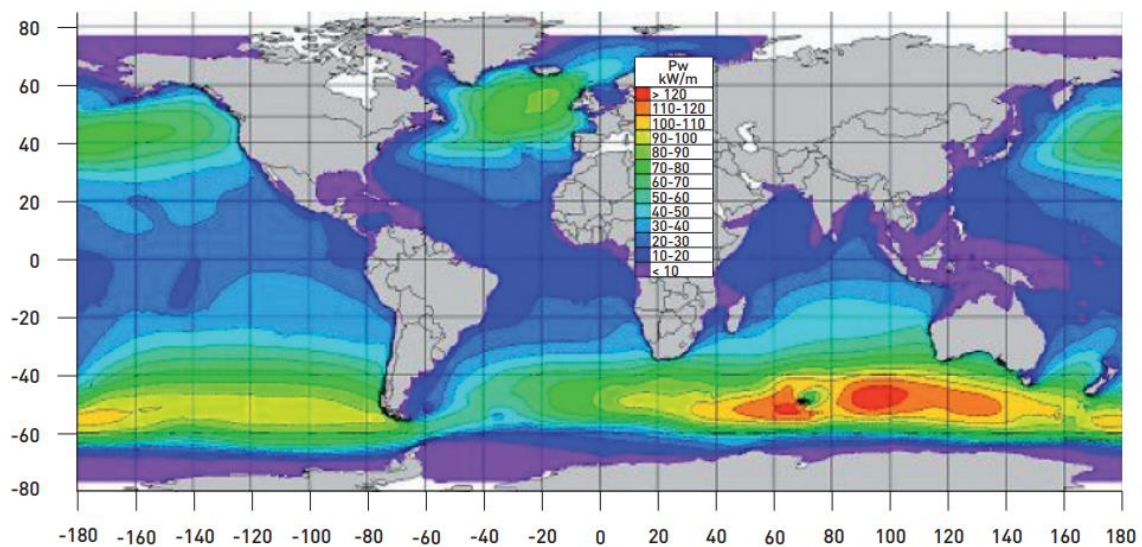


Figure 3.2. Annual wave energy distribution. Source: IDAE (2011).

Regarding to which concerns to Spain, the study realised by Losada (2011) stated that the highest potential is placed in Galicia, with mean values of 45 KW per meter of front wave, followed by coast of Cantabric Sea and Canary Islands.

However, this energy is still considered too ‘young’, it needs to experience a development to get to be competitive comparing with other energies. At present, there are many kinds of devices either in small or real scale. We can find more than 1,000 patents for Wave Energy Converters which aim to achieve a technology that permits wave energy to proof usefulness of this energy in short term. They must succeed on it while reducing environmental and social impact, and its production cost.

3.3 Wave Energy Converters

Wave Energy Converters, or WECs from now on, can be classified regarding to different terms: i) their dynamic behaviour, ii) where they are placed and, iii) the energy capture principle.

Accordinging their dynamic behaviour:

- *Actives*: The different elements of the structure move reacting to the waves and energy is obtained from the relative movement between fixed and moving parts.
- *Passives*: The structured is settled at the bottom of the sea or at the coast and energy is obtained directly from the movement water particles.

Regarding to where they are placed:

- *Onshore*: These WECs are placed on coast, next to rock cliffs, integrated in structures such as breakwaters. Always settled on the bottom of water not very deep.
- *Nearshore*: These WECs are placed in areas with a depth between 10 and 40 m, and separated some hundreds of meters from the coast. These conditions are very convenient for devices with quite a big size which lay on the bottom and for the floating ones that must be moored.
- *Offshore*: These WECs are placed in areas with a depth between 40 and 100 m. They have the hugest potential considering that they are placed on the high seas, where wave energy reaches its major potential.

Regarding the capture principle, the device follows:

- *Pressure gradient of a fluid*: These WECs take advantage of the difference of pressure produced in a fluid (typically air) by the waves. Nowadays *Oscillating Water Column (OWC)* and *Archimedes' effect* are the most popular.
- *Floating bodies*: They are made of buoyant bodies which are moved by the waves. They can convert in electricity their movement on any axis direction or rotation depending on the mechanism. On the other hand, this movement may be relative to the whole device or to any piece of it, although absolute movement are the most frequent.
- *Overflow/impact systems*: These devices can increase their kinetic or potential energy while being hit by the waves. Overflow systems force the water to go over them, while waves hit an articulated or flexible structure with the impact systems. These systems are most usually placed offshore.

In Figure 3.3 we may distinguish different WECs regarding the capture principle used by the converter.

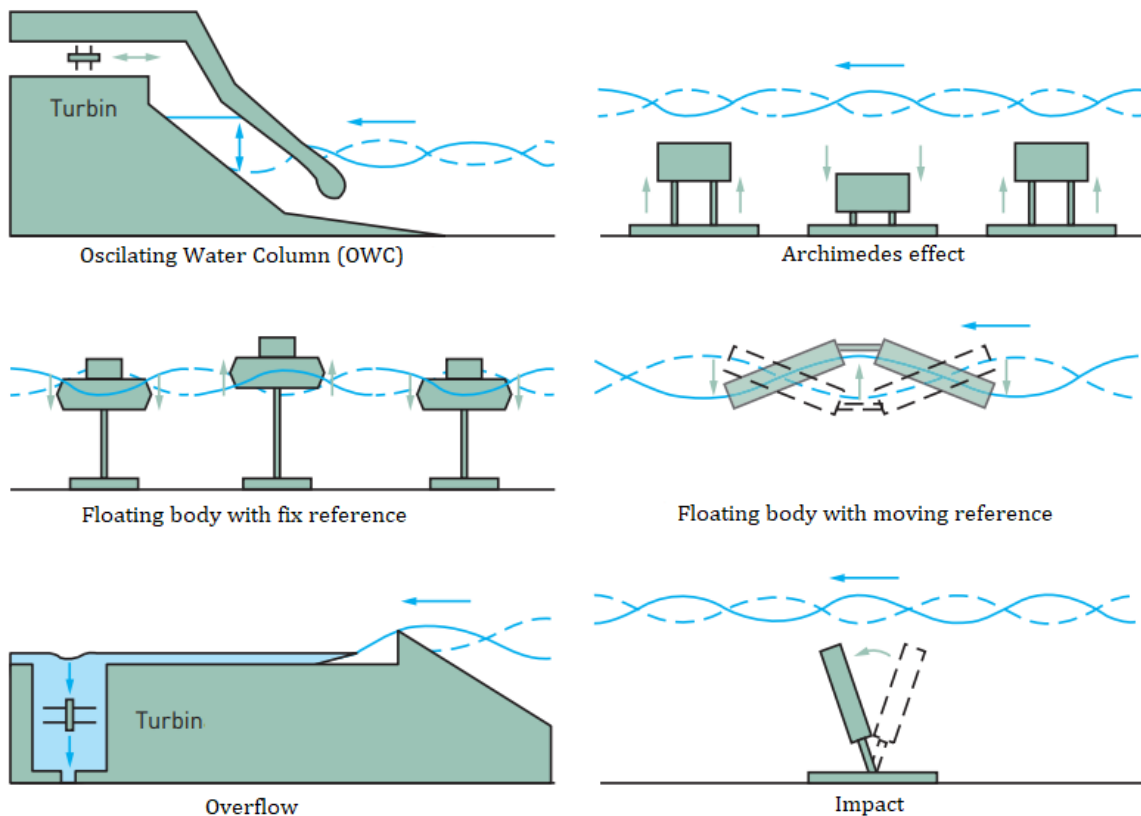


Figure 3.3. WEC types according to the capture principle.
 Source: Renewable Energies Plan 2011-2020.

3.4 FOSWEC device

The present work aims to study the Floating Oscillating Surge Wave Energy Converter, hereinafter called FOSWEC. This converter is a device structured by 2 flaps which are attached to a submerged platform. Both flaps can rotate only with 1 degree of freedom relative to the platform. The platform includes a Power Take-Off (PTO) box, which control the energy obtained by the system. The rotation of both flaps (*bow* and *aft*) interacting with the waves is used to obtain electric energy. The FOSWEC is a buoyant body due to the 4 PVC columns which form the 4 corners of a square. Each of these columns is filled with foam rubber provoking the floatability of the device. Each flap is controlled by an independent motor which constraint the 2 degrees of freedom of the system. Figure 3.4 includes some views of FOSWEC. Detailed information about the device and the experimental campaign can be found in the SAND2020-11695 report (Coe et al., 2020).

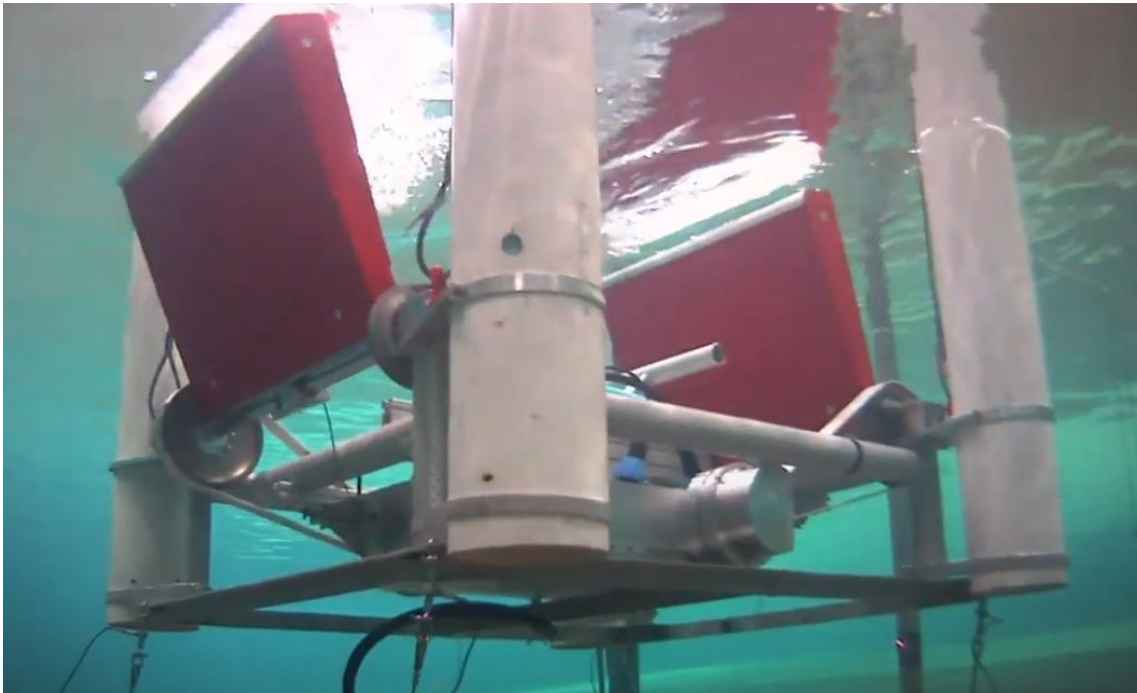


Figure 3.4. FOSWEC device. Source: <https://youtu.be/OUxbaEC2K6Y>.

FOSWEC has been developed and built by SANDIA National Laboratories in collaboration with Oregon State University. SANDIA is a multiprogram engineering and science laboratory operated by National Technology and Engineering Solution in the United States.

4. Numerical modelling

Throughout the following chapter, we will describe in detail the basis of the Smoothed Particle Hydrodynamics method (SPH), and more specifically the *DualSPHysics* code since this is the software used for our study.

During the last decades numerical modelling has stirred up every field of science. The technological growth that computers have experienced throughout the last years allows scientists to do simulations of complex systems in a reasonable time, being more and more accurate and avoiding the costs associated to the physical modelling.

The interaction between WECs and ocean waves is a complex problem. Computational Fluid Dynamics (CFD) will be then employed to simulate this phenomenon. CFD methods will consider viscous forces and high non-linear features of the wave-structure interaction. CFD are based on the integration of the *Navier-Stokes* equations, which include the continuity and momentum conservation laws:

$$\frac{\partial \rho}{\partial t} + \nabla \cdot (\rho \vec{v}) = 0 \quad (1)$$

$$\rho \left(\frac{d\vec{v}}{dt} + (\vec{v} \cdot \nabla) \vec{v} \right) = -\nabla p + \nabla f_{viscous} + \vec{f}_{ext} \quad (2)$$

where ρ is density, v is velocity vector, p is the pressure and f forces.

In order to solve these equations, we can use mesh-based or meshfree approaches. The mesh-based methods (*Finite Element Method, Volume Element Method, etc.*) have experienced a huge development during the last years, so that they provide very accurate results for a wide variety of studies. However, they require expensive mesh generation and present severe technical challenges to capturing the free surface as well as the nonlinearities within rapidly changing geometries, as it is necessary to add an algorithm that permits to know the position of the free surface at every instant and remeshing according to the movement of the geometries.

Meshfree methods are still under development, however, they have awakened an increasing interest through the past years. They can be easily applied to non-linear problems with complex geometries. Meshfree methods do not require a special algorithm to detect constantly the free surface of the fluid and, the absence of a mesh allows the method to manage simulations with significant free surface deformations obtaining accurate results.

One of the most popular meshfree methods nowadays is the SPH method (Violeau, 2012). In order to study a WEC interacting with a train of waves, it will be necessary to deal with complex geometries, floating bodies and a free surface of the fluid which will experience significant deformations. Therefore, SPH method will be a good choice for our case of study.

4.1 Smoothed Particle Hydrodynamics method

The *Smoothed Particle Hydrodynamics* method is a particle meshfree numerical model developed during the 1970s to solve problems of astrophysics. In the last decades, it has been successfully used in several studies and engineering fields (Gotoh and Khayyer, 2018).

In the SPH method the domain is discretised into a set of particles (or nodal points), where the values of the physical properties of each particle (position, velocity, density and pressure) can be obtained by local interpolation of the properties of the surrounding particles. *Navier-Stokes* equations are solved during the particle interactions and the contribution of the neighbouring particles is given using a kernel (or weighting) function, for which a smoothing length or radius of interaction will be defined.

Following, the different theoretical fundamentals of SPH will be introduced.

Kernel function

The interpolation procedure in SPH is based on the approximation of the value of a variable A placed at a point $\vec{x} \in \Omega$, where Ω is an enclosed domain in \mathbb{R}^3 , knowing the value of its surrounding points $\vec{\xi} \in \Omega$. According to this the value of the variable A placed at \vec{x} is:

$$\langle A(\vec{x}) \rangle = \int_{\Omega} W(\vec{x} - \vec{\xi}, h) A(\vec{\xi}) d\Omega(\vec{\xi}) \quad (3)$$

where W is a function called *kernel*, which depends on the distance between particles $\vec{r} = \vec{x} - \vec{\xi}$, and the smoothing length. The influence of kernel (or its radius of interaction) is usually defined as h . According to (5), the variable of integration is $\vec{\xi}$, due to the fact that we are obtaining information on a point \vec{x} knowing information in $\vec{\xi}$.

The kernel function is represented in Figure 4.1 being n a number that defines the influence of the kernel ($n=1, 2, 3$, etc).

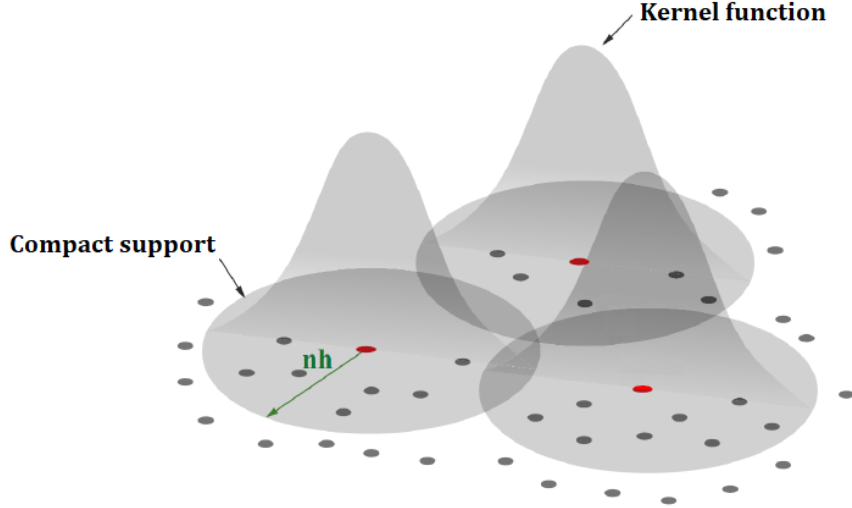


Figure 4.1. Representation of the kernel function.

The *kernel function* should verify several conditions, such as being monotonically decreasing (the more distance between particles, the less contribution), it has a compact support (particles at a distance higher than nh will not interact) and it will be continually differentiable.

In the present work, the quintic Wendland kernel (Wendland, 1995) will be used:

$$W = \begin{cases} \alpha_D \left(1 - \frac{\|\vec{r}\|}{2h}\right)^4 \left(1 + \frac{2\|\vec{r}\|}{h}\right) & 0 \leq \|\vec{r}\| \leq 2h \\ 0 & \|\vec{r}\| > 2h \end{cases} \quad (4)$$

where $n=2$, which means that *kernel* radius is $2h$ and α_D is a constant that ensures the condition of normalisation.

The expression (3) can now be translated into its discrete form using the kernel function (W). The particle of interest is denoted by i and the N neighbouring particles are denoted by j . We also consider that the volume of a particle j (V_j) can be defined as a function of its mass and density $V_j = f(m_j, \rho_j) = (m_j/\rho_j)$:

$$A_i = \sum_{j=1}^N A_j W_{ij} \frac{m_j}{\rho_j} \quad (5)$$

where $W_{ij} = W(\vec{r}_{ij}, h)$, with $\vec{r}_{ij} = \vec{r}_i - \vec{r}_j$.

Governing equations

The continuity (or mass conservation) equation of Navier-Stokes (1) can be written in SPH formalism as a summation:

$$\left(\frac{\partial \rho}{\partial t}\right)_i = \sum_{j=1}^N m_j (\vec{v}_i - \vec{v}_j) \nabla_i W_{ij} \quad (6)$$

On the other hand, *momentum conservation* equation of *Navier-Stokes* may be rewritten from (2) into discrete notation as:

$$\left(\frac{\partial \vec{v}}{\partial t}\right)_i = - \sum_{j=1}^N m_j \left(\frac{p_j}{\rho_j^2} + \frac{p_i}{\rho_i^2} \right) \nabla_i W_{ij} + \vec{g} \quad (7)$$

Equation of state

In addition to previous equations, the solver uses an equation to relate density and pressure. This equation (8) is defined as an *equation of state* and is given by the work of Monaghan (1999) and Batchelor (1974).

$$p = b \left(\left(\frac{\rho}{\rho_0} \right)^\gamma - 1 \right) \quad (8)$$

where ρ_0 is the density of reference and γ represents the polytropic index which may be considered equal to 7 for ocean applications. This means that quite small variations for density will cause a major change on pressure, that is why this approach is called weakly compressible.

According to the work of Monaghan (1994), the compressibility is adjusted in the software so that the speed of sound may be artificially lowered, which will allow the solver to set a reasonable value for the size of the time step. Nevertheless, this adjustment forces the sound speed to be at least 10 times faster than the fluid speed (at its maximum value). This is necessary because if we worked with real sound speed, we would need a size of time step very small to assure that the numerical solution could converge, which would increase significantly the running time. Keeping this in mind we can define the factor b in equation (8) as:

$$b = \frac{\rho_0 c_0^2}{\gamma} \quad (9)$$

where c_0 is equal to the sound speed when $\rho = \rho_0$.

Viscosity treatment

Viscosity plays a major role in preventing future instabilities in the simulation of the moving fluid. Therefore, viscosity effects should be added to the momentum equation (7).

The easiest way to introduce the viscosity term is the entitled as *artificial viscosity* proposed by Monaghan (1992). This is also what we have chosen to follow in the present simulations. According to this, equation (10) will be rewritten as:

$$\left(\frac{\partial \vec{v}}{\partial t}\right)_i = - \sum_{j=1}^N m_j \left(\frac{p_j}{\rho_j^2} + \frac{p_i}{\rho_i^2} + \prod_{ij} \right) \nabla_i W_{ij} + \vec{g} \quad (10)$$

where \prod_{ij} represents the term of artificial viscosity. This viscosity treatment has been applied to wave generation, propagation and interaction with coastal structures in other works (Altomare et al., 2017) providing accurate results when comparing with experimental data.

Boundary conditions

The principal purpose of the boundary conditions is to discretise solid borders and to guarantee that fluid particles will interact properly without passing through these walls. Many different approaches can be found in the SPH community, however in this work the boundary is described by a group of particles which are considered to be a set of particles different than fluid particles. This approach is named Dynamic Boundary Conditions (DBC) and full explanation can be found in Crespo et al. (2007).

The DBC approach discretises the object into boundary particles that satisfy the same equations as fluid particles, however they do not move according to the forces exerted on them. Instead, they remain either fixed in position or move according to an imposed predefined motion. When a fluid particle approaches a boundary at a distance smaller than $2h$, the density of the affected boundary particle increases, resulting in a pressure increase. This results in a repulsive force exerted on the fluid particle due to the pressure term in the momentum equation. The DBC treatment has demonstrated to work properly when applied to cases of wave propagation and wave run-up of armour block breakwaters (Zhang et al., 2018), where the interaction between fluid and boundary particles becomes critical.

4.2 DualSPHysics code

DualSPHysics (Domínguez et al., 2021) is a software based on the SPH method and developed by the group *EPhysLab* from *Universidade de Vigo*, in collaboration with *University of Manchester* (UK), *University of Parma* (Italy), *Lisbon Institute of Technology* (Portugal), *University of Ghent* (Belgium) and *New Jersey Institute of Technology* (US) – see Figure 4.2.



Figure 4.2. Institutions developing *DualSPHysics*.

Source: <https://dual.sphysics.org/developers/>.

DualSPHysics is developed to simulate free surface problems. The *EPhysLab* group is mainly focused on wave propagation and interaction between waves and fixed or floating structures (Altomare et al., 2015; Domínguez et al., 2019).

DualSPHysics is a free and open-source code and it can be download directly from <https://dual.sphysics.org/>. The code is released under the Lesser General Public Licence (LGPL), which means that the software can be incorporated into both free software and proprietary software. The LGPL license aims to encourage other researchers to have an active role on the development of the code.

The first version of the code was released in 2011 and more than 85.000 downloads have been registered in these 10 years. *DualSPHysics* can be run on the CPU (Central Processing Units) since it is developed in C++ Language, but also on GPU cards (Graphic Processing Units) thanks to its parallel programming using CUDA. The fact that the software can be executed on GPU boosted the code applications, since according to Crespo et al (2011), the GPU executions can be up to 100 times faster than the CPU ones. This allows the software to model millions of particles to perform a simulation, when a high resolution is needed, at a reasonable time of simulation.

On the other hand, the software that the user can download freely from the main website includes not only the source code of the *solver*, but also tools for *pre-processing* and *post-processing*. The *pre-processing* tools allow the user to define the geometry and the whole configuration of the case. To do it, the user will either create the input XML file or will define it through the graphic user interface (based on *FreeCad*) implemented for *DualSPHysics*. The *post-processing* codes are an important part of the software since they allow the user to analyse the results. In this way forces exerted on objects, surface elevation at different wave gauges, pressure, or velocity fields can be computed. In addition, files can be also created to visualise the simulation using free codes such as *Paraview* (<https://www.paraview.org/>).

Therefore, the full package includes all the steps as it is shown in the Figure 4.3. to create a case, run the simulation and obtain results with *DualSPHysics*.

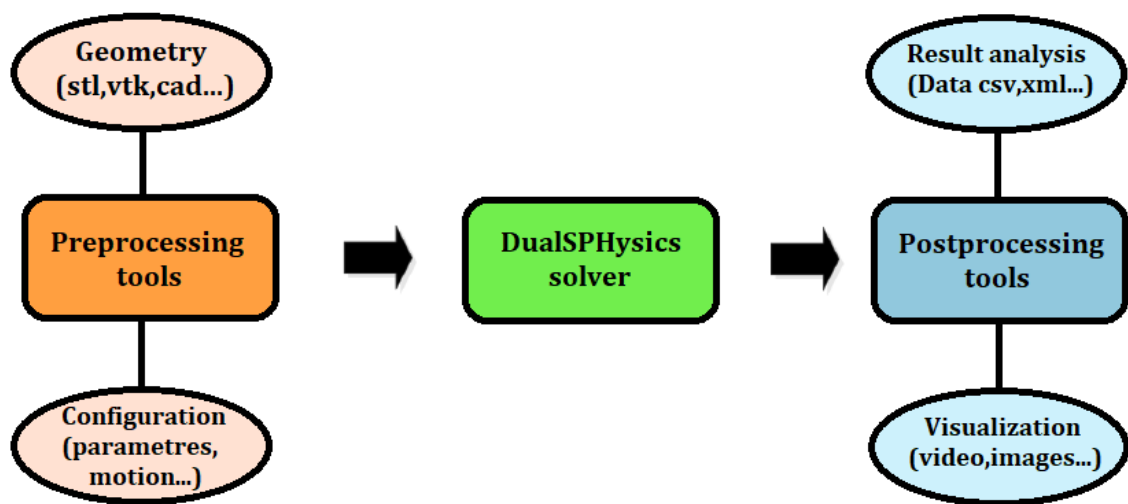


Figure 4.3. *DualSPHysics* package: *Pre-processing*, *solver* & *post-processing* tools.

4.3 Discretization with particles

Once the case is configured using the input XML file (see example in Appendix), the *pre-processing* tool named *GenCase* can be executed. One of the main purposes of *GenCase* is to discretize the geometry into fluid and boundary particles. The resolution in *DualSPHysics* (so that the number of particles) will be given by the initial distance between particles (dp). *GenCase* uses a 3-D Cartesian lattice (of dp size) to locate particles. The particles are created at the nodes of the 3-D Cartesian mesh: the mesh nodes around the object are defined and then particles are created only in the nodes needed to draw the desired geometry. Note that the geometry of the case is defined independently to the inter-particle distance. This allows the discretization of each test case with a different number of particles simply by varying the resolution (or particle size) dp . This can be observed in Figure 4.4, so that decreasing dp , we increase the number of particles, so that our case resolution.

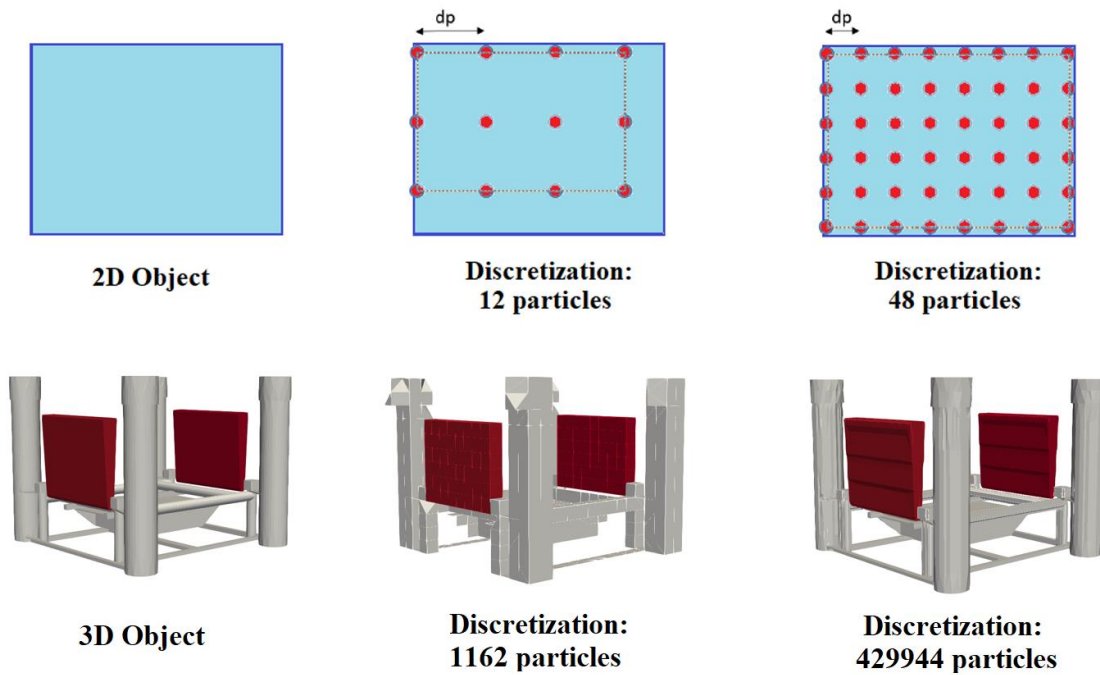


Figure 4.4. Object discretization using different resolutions.

4.4 Coupling with Project Chrono and with MoorDyn

In the present work, we aim to simulate wave energy converters that consist on a rigid body under the action of waves, where DualSPHysics is a good choice. However, the offshore floating devices will be moored to the seabed and may include a PTO (*Power Take-Off* system) that can be numerically simulated through dampers and springs.

The capabilities of the DualSPHysics package can be extended by coupling with other external libraries with more advanced functionalities as it is shown below.

Project Chrono library

As mentioned before the mechanical restrictions of the PTO system need to be simulated with accuracy. Those systems can be simulated by coupling with *Project Chrono* library.

Project Chrono is a free software, which can be freely downloaded directly from the website <https://projectchrono.org/>. This library has several applications such as robotics, mechatronics, collision detection, off-road vehicle mobility, and multibody dynamics. The latter ones allow user to run simulations of mechanisms made of rigid bodies, so that we can apply constraints to parts using a wide set of joints, motors, linear actuators, springs and dampers. In the particular case of FOSWEC, this library will allow us to simulate the hinges that link both flaps to the buoyant platform and the experimental properties of the hinges (damping and stiffness coefficients) will be defined in the simulation. Therefore, the forces and torques are numerically solved using a coupling between *DualSPHysics* and *Project Chrono*. More information about the coupling procedure can be found in Canelas et al. (2018).

MoorDyn Library

In our case of study, the FOSWEC is attached to the bottom by four taut mooring lines, which limit the movement of the WEC (mainly heave, surge and pitch rotation). These mooring lines will exert an extra force applied to the device that needs to be simulated accurately. This is why, the *MoorDyn* library is also coupled with *DualSPHysics*.

MoorDyn is an open source-code that can be obtained for free from <http://www.matt-hall.ca/moordyn.html>. This library can solve the dynamic of the mooring system and it has been developed in order to be coupled with other software. To compute the mooring tensions, *MoorDyn* discretizes the lines as punctual masses linked by linear models, for modelling certain elasticity in the axial direction of the mooring. The model also solves the friction that the moorings have with the bottom. *MoorDyn* has proved, with a very simple formulation, that it is computationally efficient and accurate to simulate floating bodies with moorings under regular waves (Domínguez et al., 2019).

Figure 4.5 includes the flow chart of the coupling of *DualSPHysics* with *Project Chrono* and with *MoorDyn* libraries. The main idea is that the interaction between waves a floating rigid bodies is mainly solved by *DualSPHysics*. However if collisions or mechanical restrictions (as in the case of the PTO of FOSWEC) need to be considered, then *Project Chrono* will compute forces and torques at each time step and will solve the new position of the rigid body considering all forces acting on it (fluid-body forces and mechanical restrictions). In addition, if mooring lines are attached to the floating body, *MoorDyn* is used to obtain the forces on the fairleads and *DualSPHysics* will finally solve the motion of the body.

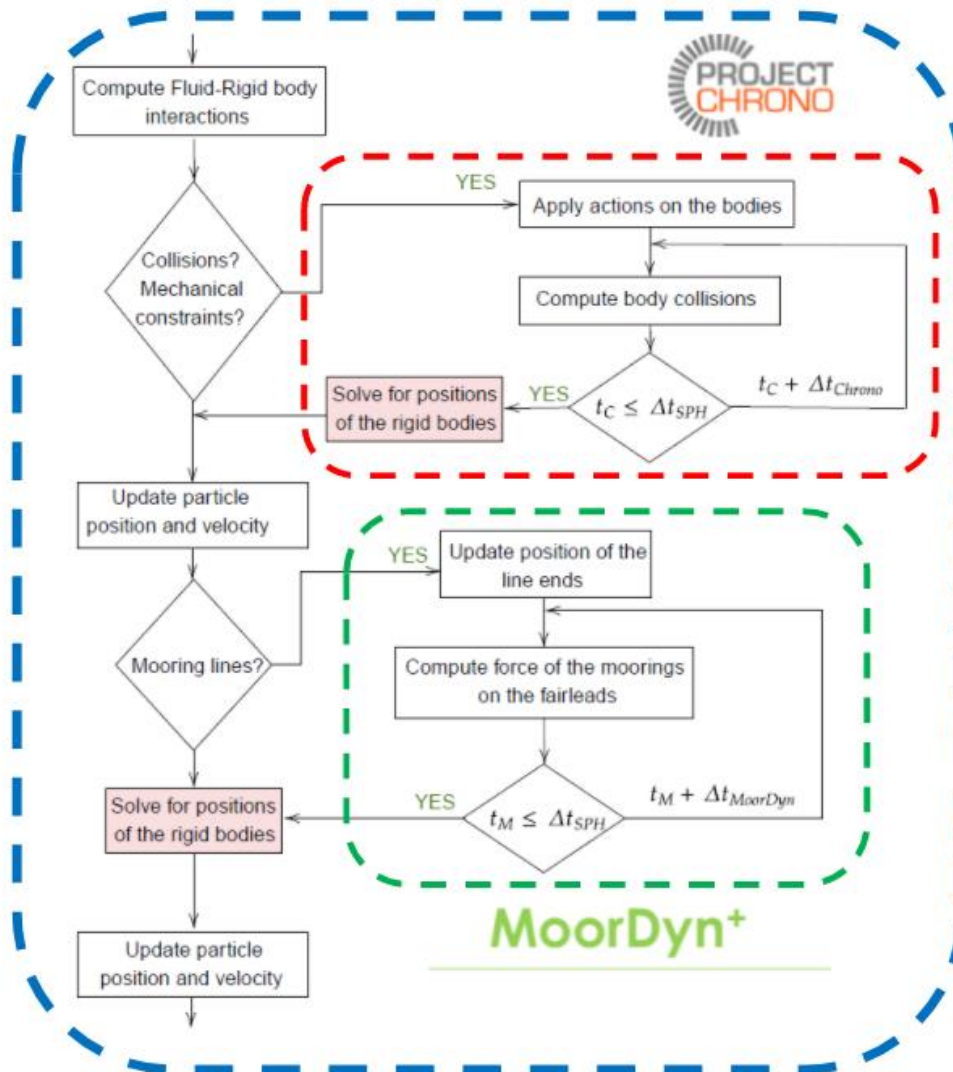


Figure 4.5. Flow chart of the coupling of *DualSPHysics* with *Project Chrono* and with *MoorDyn*.

5. Validation

The main goal of this chapter is to prove the capabilities of the SPH method to reproduce the hydrodynamic response of the FOSWEC device. To do this, it is necessary to assure that the software *DualSPHysics* obtains accurate results comparing to experimental results.

To perform a validation, we will recreate the exact same conditions as the ones in the actual experiment. Therefore, the first task is to make sure that our numerical setup is capable to reproduce, propagate and absorb properly the numerical waves, contrasting with the theoretical results. Once the correct wave propagation is confirmed, the floating moored FOSWEC will be introduced in the numerical model with the same conditions and properties described during the physical experiment. Next, the simulation will be run, and numerical results will be compared with the experimental ones in terms of: i) motions of the hull, ii) tensions in the mooring lines and iii) motions of the flaps.

5.1 Experimental configuration

SANDIA National Laboratories has developed the FOSWEC and has analysed its response in their facilities in the United States. The company placed the device in a huge wave pool (*Directional Wave Basin*) where they could create different conditions of regular and irregular waves and set different values of damping and stiffness at the hinge of the flaps.

SANDIA aimed to obtain a large set of values with the less measuring error the better so they decided to subject the FOSWEC to a certain type of regular waves for a certain time. Once this time was over, they modified the movement of the piston so the FOSWEC would be under the action of regular waves of other conditions. The different wave conditions are defined using different values of the wave height and wave frequency as shown in Table 5.1.

Table 5.1. Different conditions of the regular waves.

		Wave Height [m]				
		0.015	0.045	0.136	0.250	0.400
Wave Frequency [Hz]	0.19	R1A	R1B	R1C	R1D	R1E
	0.26	R2A	R2B	R2C	R2D	R2E
	0.38	R3A	R3B	R3C	R3D	R3E
	0.51	R4A	R4B	R4C	R4D	R4E
	0.64	R5A	R5B	R5C	R5D	R5E
	0.80	R6A	R6B	R6C	R6D	R6E

In the present work, only one wave condition shown in the table will be reproduced using the numerical model *DualSPHysics*. The case R5C was chosen, since its simulation will take less runtime than other cases due to its wavelength (to be explained further in this document).

The dimensions of the *Directional Wave Basin* are 48.8 m long and 26.5 m wide, with adjustable depth (defined as 1.36 m for the R5C test). According to Figure 5.1, the FOSWEC device will be placed in the longitudinal centre line of the pool and almost 17 m away from what it is considered as the origin of the wave basin. In the figure, the FOSWEC is represented as an orange rectangle and the position of several wave gauges (resistive and acoustic) are indicated.

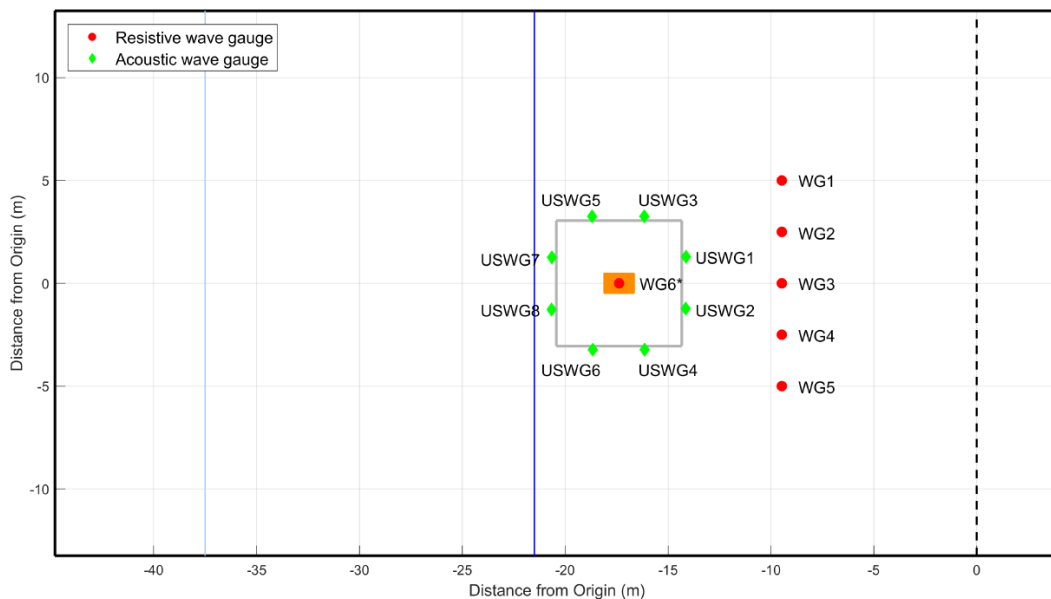


Figure 5.1. Dimensions of the wave basin and location of FOSWEC and the wave gauges during the experimental campaign.

Figure 5.2 includes the dimensions and parts of the FOSWEC2 device that has a height of 1.275 m, a width of 1.65 m and length of 1.54 m. It includes a central platform (or hull) of 276 kg and two flaps (brown colour in the figure) of 6 kg each one. The two flaps are hinged to pivot about shafts mounted to the hull and are controlled by independent motors. Buoyancy of FOSWEC is provided by four vertical PVC spars on the corners of the device. The system is also set so that the highest part of both flaps is placed 2 cm below the free surface, almost at the same level. In addition, the hull of the device is attached to the bottom by four mooring taut vertical lines of the same length (0.34 m). This particular configuration of the mooring lines allows certain surge in presence of the waves and limit the heave movement. In this way, designers have boosted the flap movement, and hence energy production.

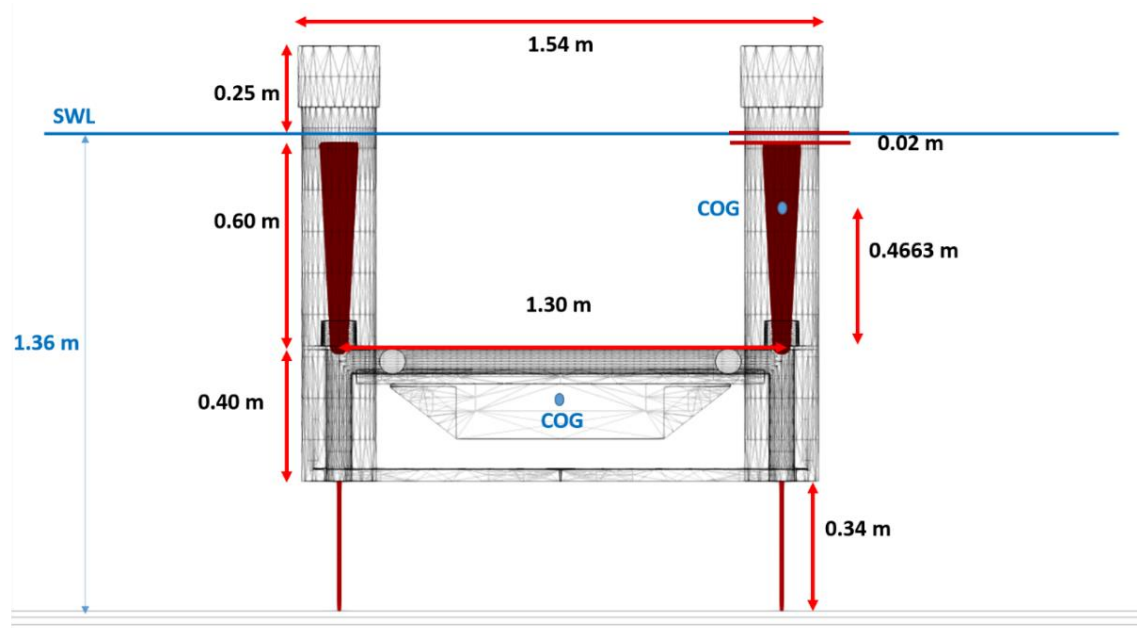


Figure 5.2. FOSWEC dimensions.

5.2 Numerical setup

This section will include details of the numerical tanks dimensions, information of the rigid bodies that form FOSWEC, definition of the PTO system and features of the mooring lines.

First, we need to define a numerical setup that reproduce the same conditions given in the real experiment. However, as we will be using a software such as *DualSPHysics* it would not be feasible to reproduce exactly the same tank that SANDIA used in the experimental campaign, since a tank of those dimensions will imply enormous computational times. So instead of an exact reproduction of the wave basin we will configure a smaller numerical tank that can reproduce the same conditions and reduce the runtime.

The test R5C from Table 5.1 will be considered so the numerical tank includes an initial water depth (d) of 1.36 m and a piston that will generate waves 0.136 m high (H) and wave period (T) of 1.5625 s (the inverse of the frequency of 0.64 Hz). To guarantee a proper wave generation and propagation at the FOSWEC position, the device needs to be located at one wavelength (L) away from the piston. For the target wave condition, $L=3.73$ m. Table 5.2 collects all these wave parameters.

Table 5.2. Wave conditions of experimental setup R5C.

Parameter	Value
Wave period, T	1.5625 s
Wave height, H	0.136 m
Initial depth, d	1.36 m
Wavelength, L	3.73416 m

The numerical wave tank is represented in Figure 5.3 (top and lateral view). As mentioned before, the WEC is located at one wavelength from the piston. A dissipative beach is also located after the WEC position, in particular, $L/4$ away from the device. The main objective of this beach is to avoid the wave reflection in the tank so that the device is always under the action of the target incident regular wave condition during the complete simulation. Regarding the transversal direction (width of the tank), FOSWEC is placed at mid position and it is necessary to leave some lateral space between the object and the walls of the tank in order to avoid the lateral reflection. In our case, it has been proven that using a tank two times wider than the WEC width is enough to avoid reflection since the flap is a moving body and it is less likely to produce too much reflection.

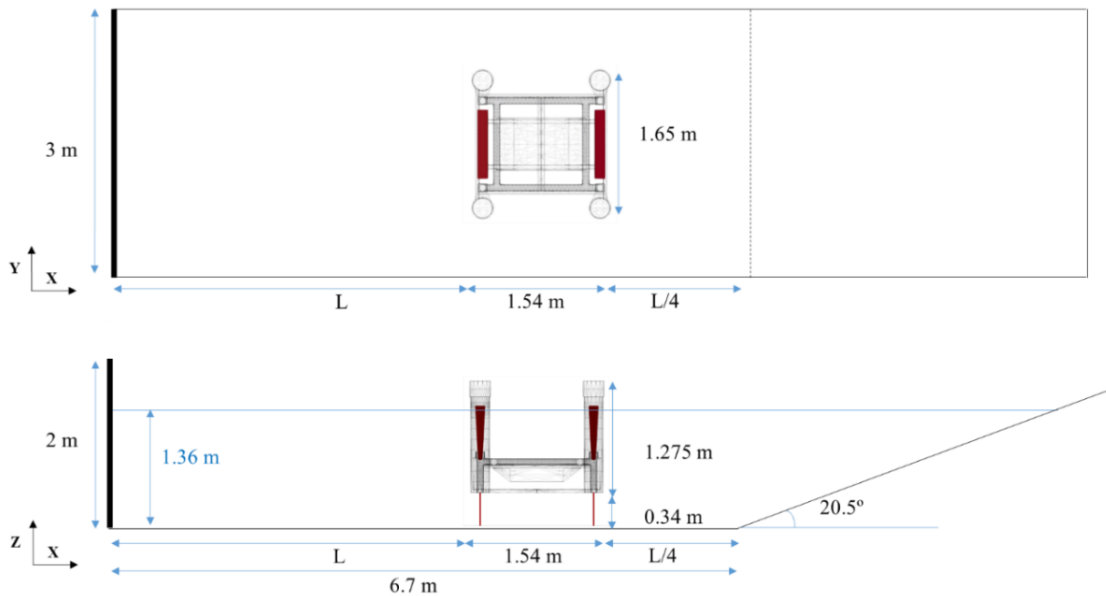


Figure 5.3. Numerical wave tank for R5C (top and lateral view).

To summarize, we have configured the numerical tank shown in Figure 5.3 in order to minimise the runtime of the simulations, reducing phenomena like reflection (discussed in the following section) and hence registering the same wave conditions as in the actual experiments performed by SANDIA.

Once the dimensions of the numerical tank are defined, it is very important to consider the actual mass, centre of gravity (COG) and moments of inertia of the hull and the flaps according to the experimental information. The values of these important magnitudes are summarised in Table 5.3. COG was already represented in Figure 5.2 and it is defined considering $X=0$ at the piston position, $Y=0$ in middle of the tank width and $Z=0$ at initial water surface.

Table 5.3. Features of the floating parts of FOSWEC.

Parameter	Value
Mass of the hull	276 kg
COG (X,Y,Z) of the hull	(4.51, 0, -0.7296) m
Inertia (I_{XX}, I_{YY}, I_{ZZ}) of the hull	(43.46, 49.36, 77.75) kg·m ²
Mass of the flap	6 kg
COG (X,Y,Z) of the flap	(3.86, 0, -0.1537) // (5.16, 0, -0.1537) m
Inertia (I_{XX}, I_{YY}, I_{ZZ}) of the flap	(0.61, 0.31, 0.31) kg·m ²

The PTO system introduced in the R5C test includes stiffness and damping at the bow and aft flaps following the values of Table 5.4. These coefficients will be defined in the configuration of the hinge in the *Project Chrono* library.

Table 5.4. Stiffness and damping coefficients of the PTO system.

Parameter	Value
Stiffness coefficient of the bow flap	-3.561 N·m/rad
Damping coefficient of the bow flap	1.762 N·m·s/rad
Stiffness coefficient of the aft flap	2.800 N·m/rad
Damping coefficient of the aft flap	0.4654 N·m·s/rad

Finally, the information about mooring lines are configured to use the *MoorDyn* library. The four lines were cables made of steel and their features are included in Table 5.5.

Table 5.5. Information about the four mooring lines.

Parameter	Value
Length	0.34 m
Volume equivalent diameter	0.0035 m
Mass per unit length	0.07 kg/m
Stiffness (steel)	$8.315 \cdot 10^9$ N/m ²

The simulations are performed for different numerical resolutions. As explained in the section 4.3, the resolution in the *DualSPHysics* code is given by the initial particle distance, dp . A total physical time of 14 seconds are simulated for $dp=0.05, 0.02, 0.01$ m using a GPU card (GeForce RTX 2080 Ti) as the execution device. This GPU card is available at the *Data Processing Centre* (CPD) managed by the *EPhysLab* group. Table 5.6 includes the number of particles and the runtime for each resolution. It can be observed how decreasing dp , the number of particles (Np) increase, so that the runtime.

Table 5.6. Resolution, number of particles and runtime.

dp [m]	Np ($\cdot 10^6$)	Runtime
0.05	0.335	27.6 min
0.02	4.777	7 hours
0.01	36.751	5 days

5.3 Wave generation, propagation and absorption

The second order wave generation theory implemented in *DualSPHysics* is based on Madsen (1971) who developed a simple second-order wavemaker theory to generate long second order Stokes waves that would not change shape as they propagated. The wave conditions to generate in the test R5C (Table 5.2) correspond to second order so that they will be generated using *DualSPHysics* in an automatic way.

As it was mentioned in the previous section, reflection is a major issue to deal with if we are aiming to reproduce the behaviour of the FOSWEC in presence of regular waves, since it is mandatory to assure that the target incident waves reach the position of the device. In order to verify that the waves are propagating properly and that the reflection is avoided, we will compare the results obtained with the SPH method with the results obtained in the experiment by SANDIA.

In order to avoid reflection at the end of the numerical tank, a dissipative beach was added at the end (as shown in Figure 5.3) and a *damping* zone is also defined for the extension of the beach. The *damping* tool implemented in *DualSPHysics* (according to Altomare et al., 2017) allows us to gradually decelerate the moving fluid particles that enter this *damping zone* (Figure 5.4).

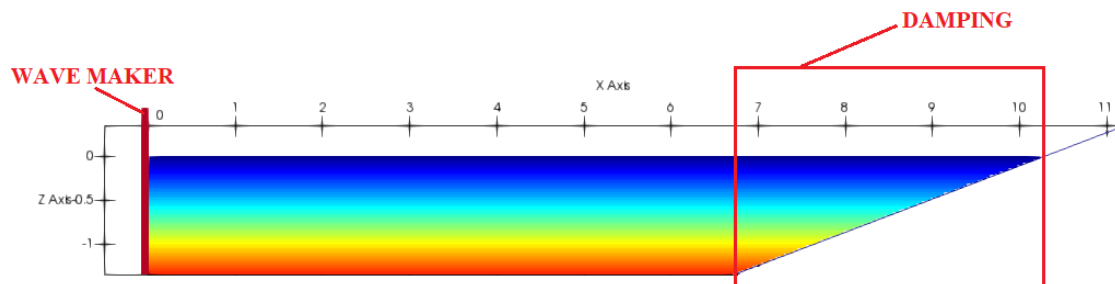


Figure 5.4. Piston wavemaker and damping zone in the numerical tank designed for wave generation and propagation.

Remember that the experimental wave basin was 26.5 m wide and the numerical tank is only 3 m wide. Therefore, a lateral periodicity condition has been also applied to configure the numerical tank. The periodicity condition links particles close to the edges from both lateral walls so that they complete each other the compact support for particle interactions from both edges. This means that no boundary walls are created, so that we avoid numerical friction in those lateral limits.

Several instants of the simulation with $dp=0.02$ m and without the device in the numerical flume are depicted in Figure 5.5, where colour of the particles corresponds to the longitudinal velocity. The time window showed in this figure corresponds almost to one complete period ($T=1.5625$ s), so that the first and the last frame are pretty much equal. It is also observed that the maximum positive and negative velocity values are registered for particles at highest (valleys) and the lowest (crests) surface elevations, respectively.

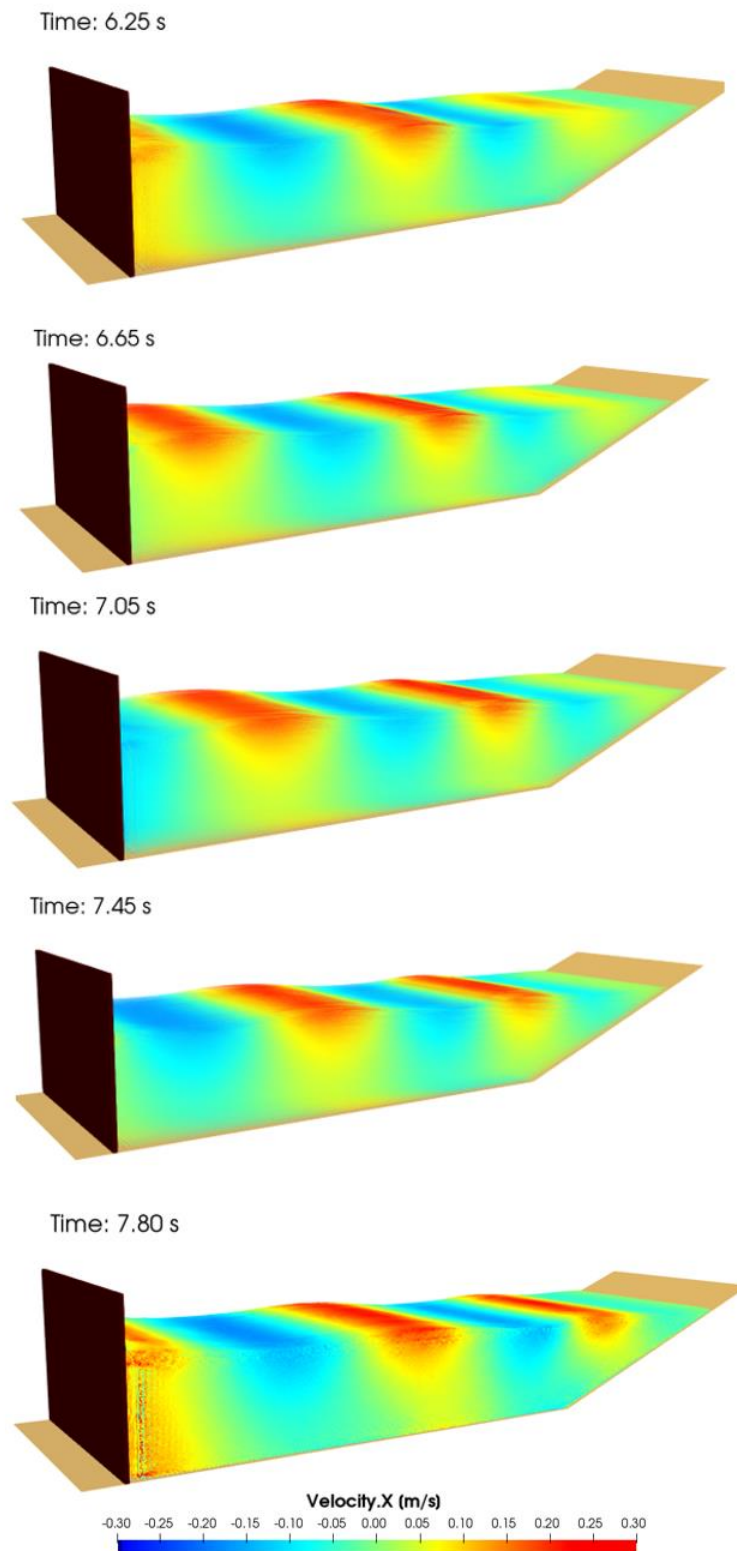


Figure 5.5. Different instants of the wave propagation during a period ($d_p=0.02$ m).

Now the experimental data measured by SANDIA is compared with the results obtained numerically for the three different resolutions (dp). As it was shown in Figure 5.1, the experimental resistive wave gauge $WG6$ was placed at the FOSWEC location. SANDIA placed this gauge there to verify that they obtained the desired wave before testing the device. Once this was verified, they removed that gauge and they placed the FOSWEC in that position (Figure 5.1). Therefore, the validation of the numerical wave propagation is carried out by comparing the SPH results (for the 3 values of dp) with the experimental data from $WG6$ gauge in Figure 5.6. It can be seen that higher resolution leads to a better agreement with the experimental time series. In fact, the results with $dp=0.02$ m looks accurate enough.

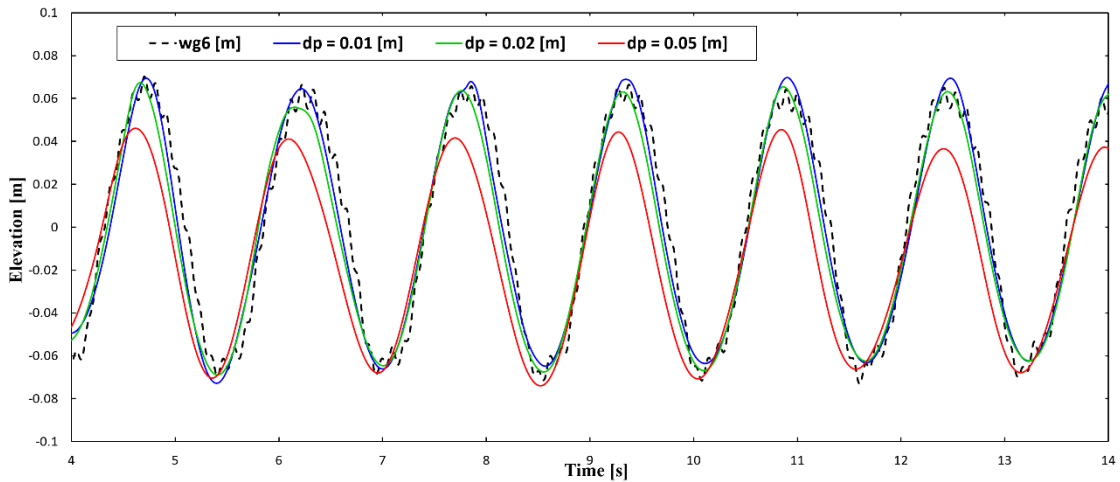


Figure 5.6. Time series of experimental and numerical free-surface elevation.

The reflection coefficient, K_r , can be obtained through the *Healy* method (Eagleson and Dean (1966)) by:

$$K_r = \frac{H_{max} - H_{min}}{H_{max} + H_{min}} \quad (11)$$

where H is the wave height amplitude. The K_r obtained for all the simulations (three values of dp) are below 2.5 %, which means that the dissipative beach and the damping zone are absorbing over 97.5 % of the incident waves. Therefore, we can conclude that there is no significant reflection in our tank configuration and the target waves are being generated and propagated in an accurate way in our numerical domain.

5.4 Motions of the hull

The FOSWEC has been introduced in the numerical tank described in previous sections, at one wave length away from the piston. Some instants of the interaction of the device with the regular waves of test R5C are shown in Figure 5.7. Colour of the particles corresponds to the values of the longitudinal velocity field.

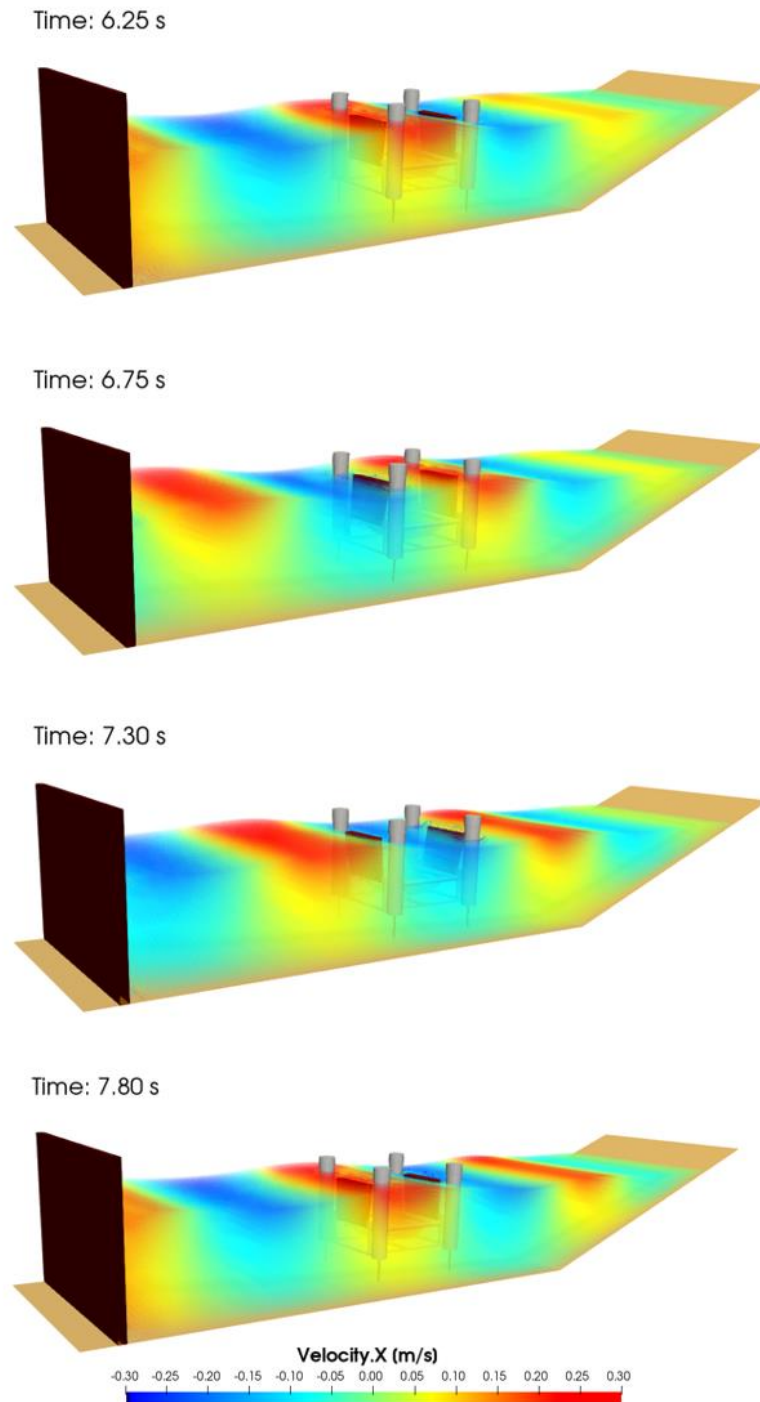


Figure 5.7. Different instants of the interaction between regular waves and FOSWEC during a period ($d_p=0.02$ m).

The following Figure 5.8 displays the heave, surge and pitch angles of the hull registered during the experiment and computed using *DualSPHysics*. The simulations were executed for $dp=0.05$ m, 0.02 m 0.01 m. It can be observed in the figure, there is a good concordance between the SPH results and experimental ones, noticing that it does not exist a great difference between $dp=0.01$ m and $dp=0.02$ m.

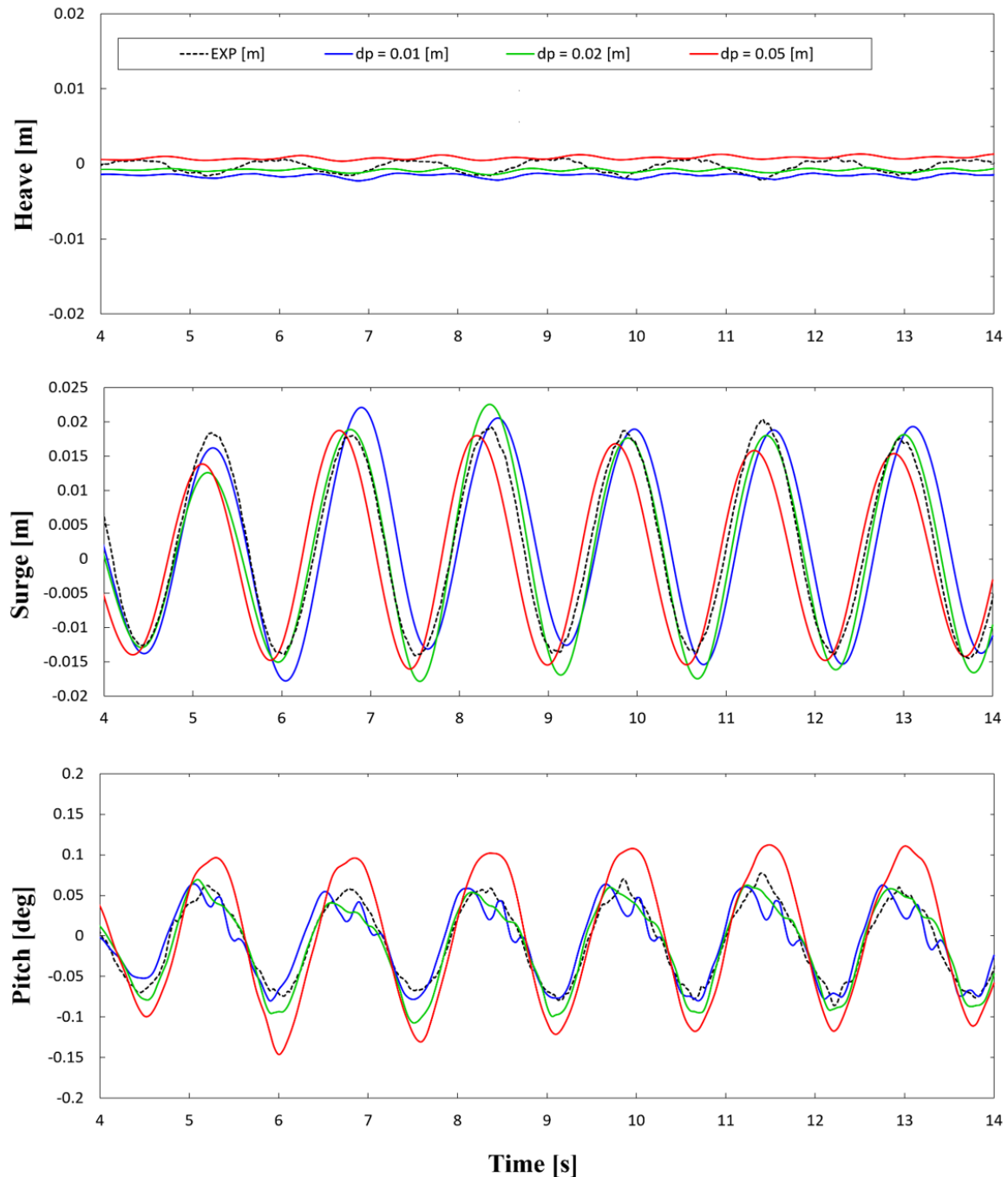


Figure 5.8. Time series of experimental and numerical heave, surge and pitch.

5.5 Mooring tensions

This section aims to validate, mainly, the coupling between *DualSPHysics* and the *MoorDyn* library. Previous section shows that motions of the hull (heave, surge and pitch) were in agreement with experimental data, which also proves that the four mooring lines limit the heave motion and restrict the surge motion and pitch angles. The *MoorDyn* library is configured using the experimental information provided about the mooring lines and its material (Table 5.5).

The experimental values of tension are compared with the numerical results computed by the *MoorDyn* library. Since FOSWEC is a symmetric device and the wave, that arrives in the direction of the axis of symmetry, is also symmetric; it will only be necessary to display time series of two moorings (bow and aft), since the other two will manifest the same results. A comparison between the experimental and numerical tensions (for the three different resolutions) is shown in Figure 5.9.

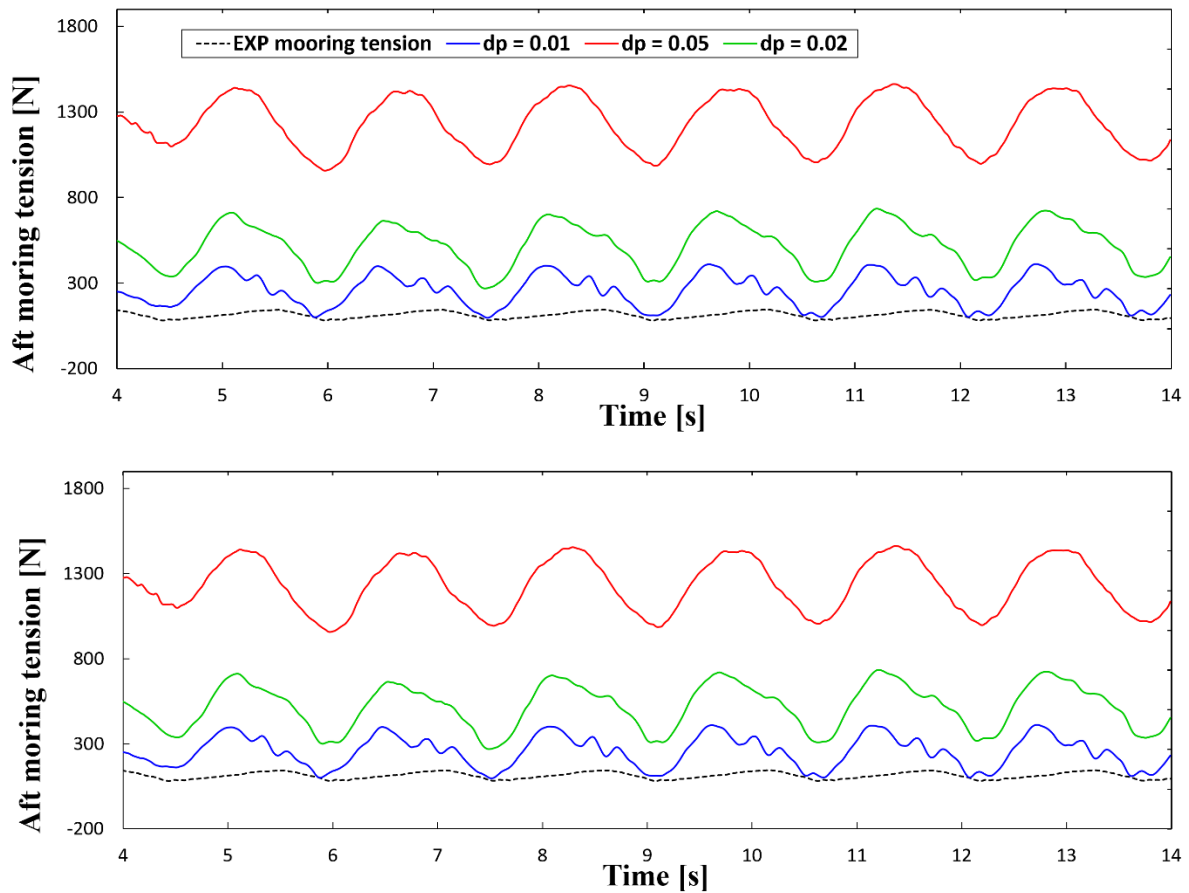


Figure 5.9. Time series of experimental and numerical mooring tensions.

Figure 5.9 evinces that the results obtained by SPH are not the desired ones since they manifest a significant difference with the results reached in the basin during the experiments. This can be attributed to the fact that the resolution used for these simulations may be insufficient to validate the tension values.

An object which tends to float requires a tension restraint force T in order to remain submerged. In this case the initial pretension in the mooring lines (Figure 5.9) result from the buoyant force experienced by the floating WEC minus the weight following:

$$T = \rho_{fluid} \cdot g \cdot V - M \cdot g \quad (12)$$

where ρ_{fluid} is the density of the fluid, g the gravity acceleration constant, V is the submerged volume of the body and M is the actual mass of the object. In *DualSPHysics*, we have introduced the actual mass (M) of the FOSWEC (Table 5.3) as it was given in the experimental report. Therefore, the exact volume of the FOSWEC (V) needs to be properly considered in the numerical simulations. *DualSPHysics* will consider the volume of the device by approximating its volume to the volume of the particles that discretizes it. The smaller dp we use for a simulation, the higher amount of particles will be used to discretize the FOSWEC geometry and hence the numerical volume will be more accurate and closer to the actual one (V). This dependence with resolution can be easily seen in Figure 5.10, that shows the discretization of the FOSWEC device for different values of dp (0.05, 0.02, 0.01, 0.005 m).

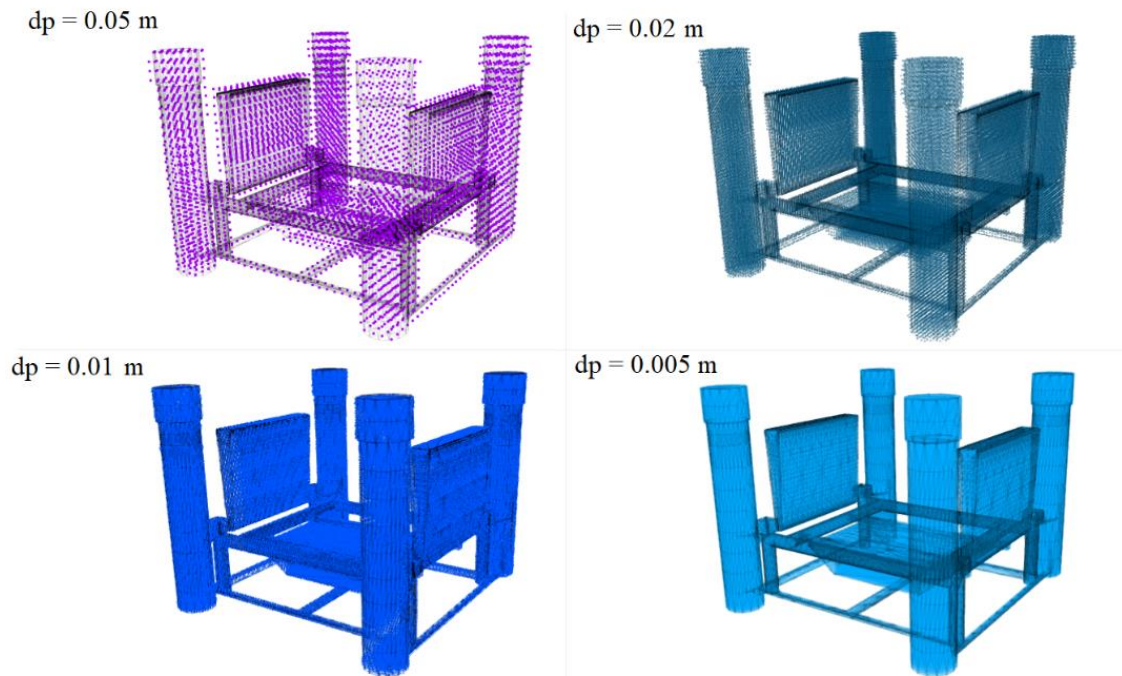


Figure 5.10. Particle discretization of the FOSWEC device for different resolutions.

In order to prove this issue of the resolution affecting the buoyant force and so the initial mooring tensions, a new case with the FOSWEC structure and the moorings at still water has been analysed. The objective of these extra simulations is to prove that for smaller values of dp , it will be possible to reach the experimental tension values in the mooring cables.

We have performed these simulations with a reduced box filled with still water since higher resolutions imply much more particles and therefore a significant increase on the runtime. The results are shown in Figure 5.11, where the experimental tensions before the waves arrival (so that with the device at rest) are compared with numerical tensions using different resolutions ($dp= 0.05, 0.02, 0.01$ m) and including a new one of 0.005 m, which reaches a very accurate result.

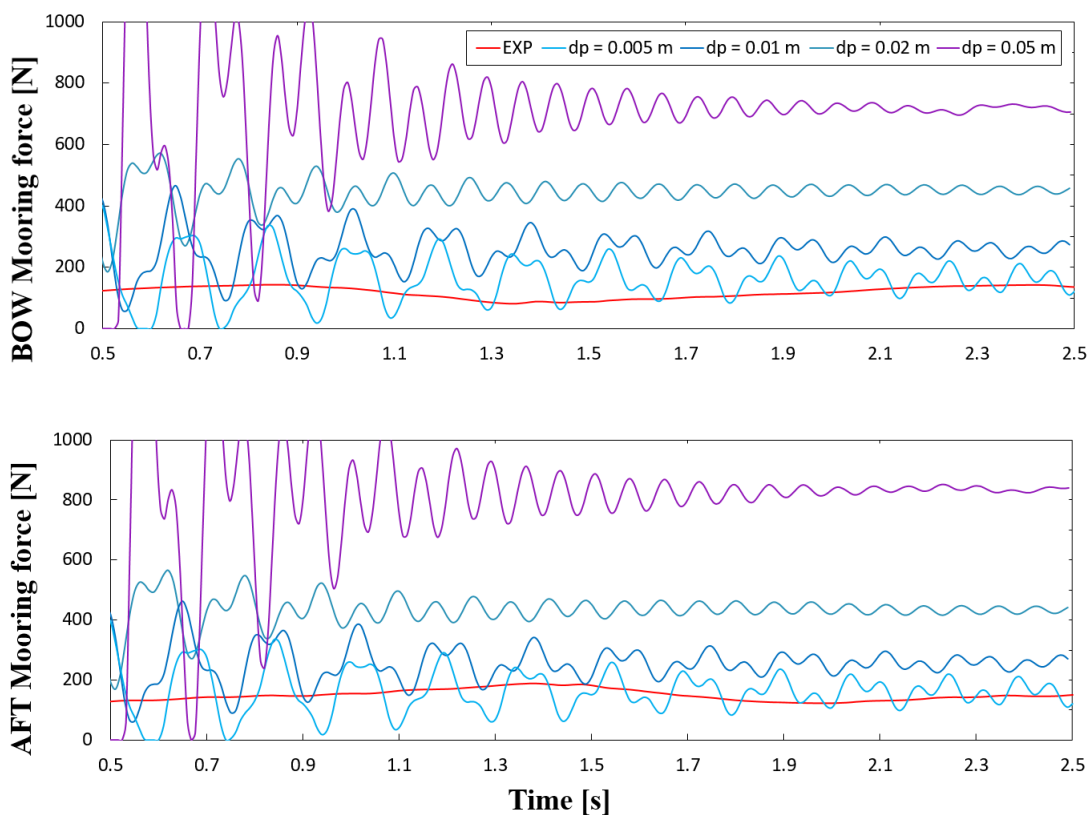


Figure 5.11. Time series of experimental and numerical mooring tensions for different resolutions obtained in the still water test.

It has already been shown in previous section, that the numerical results using $dp=0.02$ m and $dp=0.01$ m provide accurate results in terms of the motion of the hull. Considering this, and the fact that reducing the dp to 0.005 m will lead to enormous computational runtimes, it has been decided to keep working with numerical results of the initial resolutions.

5.6 Motions of the flaps

Once the motions of the hull have been validated, the motion of both flaps need to be evaluated (for the different resolutions defined from the beginning).

The coupling with the *Project Chrono* library will restrict the movement of the flaps, performing the role of a physical hinge. The PTO system will be modelled according to the next equation that defines the torque applied along the axis of the hinge:

$$T_{PTO}(t) = -k_{PTO}\theta(t) - b_{PTO}\dot{\theta}(t) \quad (13)$$

where k_{PTO} is the torsional stiffness, b_{PTO} is the torsional damping, θ is the flap angle of rotation and $\dot{\theta}$ is the angular velocity of the flap. The values of stiffness and damping for the bow and aft flap during the experiment are the ones reported in Table 5.4.

The comparison between the experimental flap angles and the angles during the SPH simulations is displayed in Figure 5.12. It can be noted that the agreement for the three different resolutions is good enough, which proves the accuracy of the model to flap motions.

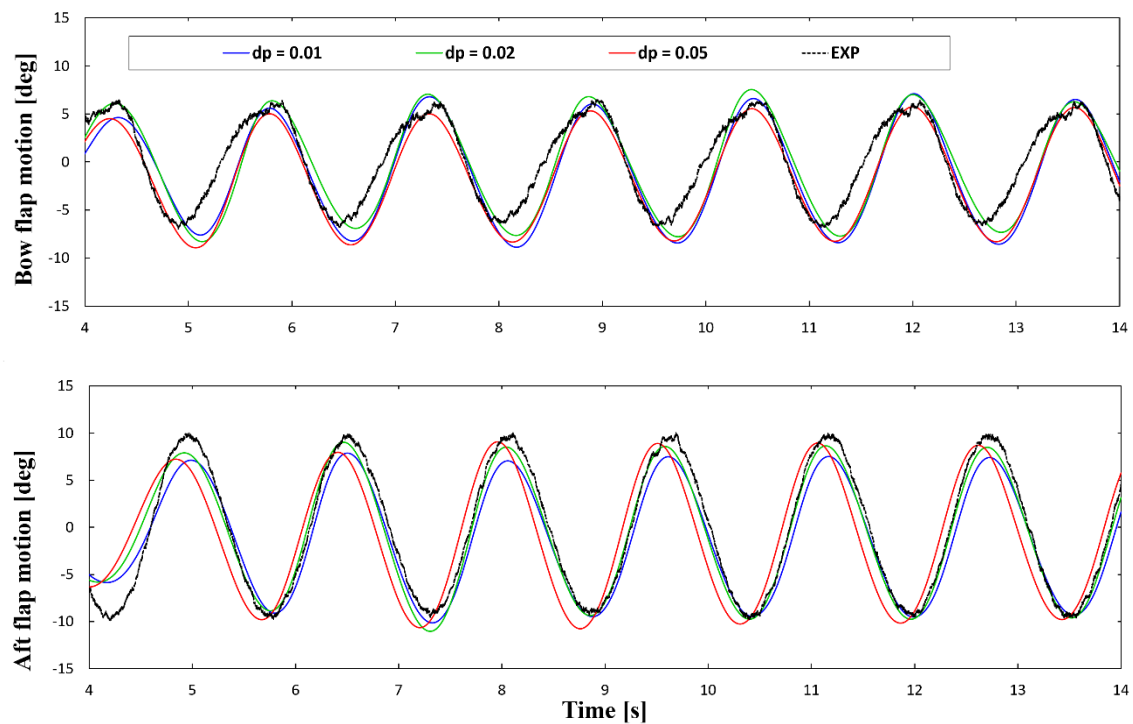


Figure 5.12. Time series of experimental and numerical angles of bow and aft flaps.

The numerical results shown in the last sections and the good agreement with the experimental data prove the capabilities of the *DualSPHysics* code (coupled with *MoorDyn* and *Project Chrono*) to study the hydrodynamic response of a complex system such as the FOSWEC device under the action of regular waves.

6. Efficiency analysis

This chapter will show how the efficiency of WECs can be computed. In particular, the efficiency for the FOSWEC device will be obtained for the wave condition analysed in the previous chapter of validation, but also the efficiency is analysed for a different range of wave periods and PTO systems.

6.1 Power computation

The available wave power per meter of width can be computed for the wave front as:

$$J = \frac{1}{16} \rho g H^2 \frac{\omega}{k} \left[1 + \frac{2kd}{\sinh(2kd)} \right] \quad (14)$$

with $\omega=2\pi/T$ defined as the angular velocity and $k=2\pi/L$, the wave number.

The total width of wave front that interacts with the device is equal to the characteristic width (D), so that the wave power, P_w , that can be absorbed by the device will be:

$$P_w = JD \quad (15)$$

Let us now define the absorbed power by the device. The FOSWEC device consists of two flaps that are hinged to pivot about shafts mounted to a central platform. Therefore, the characteristic width D is the width of the flap in this case. The two flaps are driven by two identical belt drive systems with a 3.75:1 gear ratio. Therefore, the PTO system can be numerically simulated as the torque exerted on the gear, that will follow the expression:

$$T_{PTO}(t) = k_{PTO}\theta(t) + b_{PTO}\dot{\theta}(t) \quad (16)$$

where k_{PTO} is the stiffness (in Nm/rad), b_{PTO} is the damping (in Nms/rad), θ is the flap angle (in rad) and $\dot{\theta}$ is the angular velocity (in rad/s). Therefore the torque here is divided into an elastic component ($k_{PTO}\theta$) and a viscous component ($b_{PTO}\dot{\theta}$).

The energy harvested by the device is taken from the motion and defined as the dissipated viscous force, so that the power absorbed by this PTO system will be determined by:

$$P_a(t) = b_{PTO}\dot{\theta}(t) \cdot \frac{d\theta(t)}{dt} = b_{PTO}\dot{\theta}^2(t) \quad (17)$$

The integral of Eq. (16) over a time period (T) will give us the averaged power absorbed by the device:

$$P_a = \frac{1}{T} \int_{t_0}^{t_0+T} P_a(t) dt \quad (18)$$

Therefore, we will here define the efficiency using the Capture Width Ratio (CWR) parameter that can be obtained as

$$CWR = \frac{P_{a,bow} + P_{a,aft}}{P_w} \quad (19)$$

6.2 Results for the validation case

Let us start computing the efficiency achieved by the FOSWEC device in the physical test R5C, which is the test chosen to conduct the validation presented in the chapter 5.

In order to determine the absorbed power, the magnitude of interest is the angular velocity of the two flaps (bow and aft), that is represented in Figure 6.1. The time series of the simulations with different resolutions ($dp=0.05$, 0.02 and 0.01 m) are included in the figure and it can be observed that values of the two highest resolution converged to the same result.

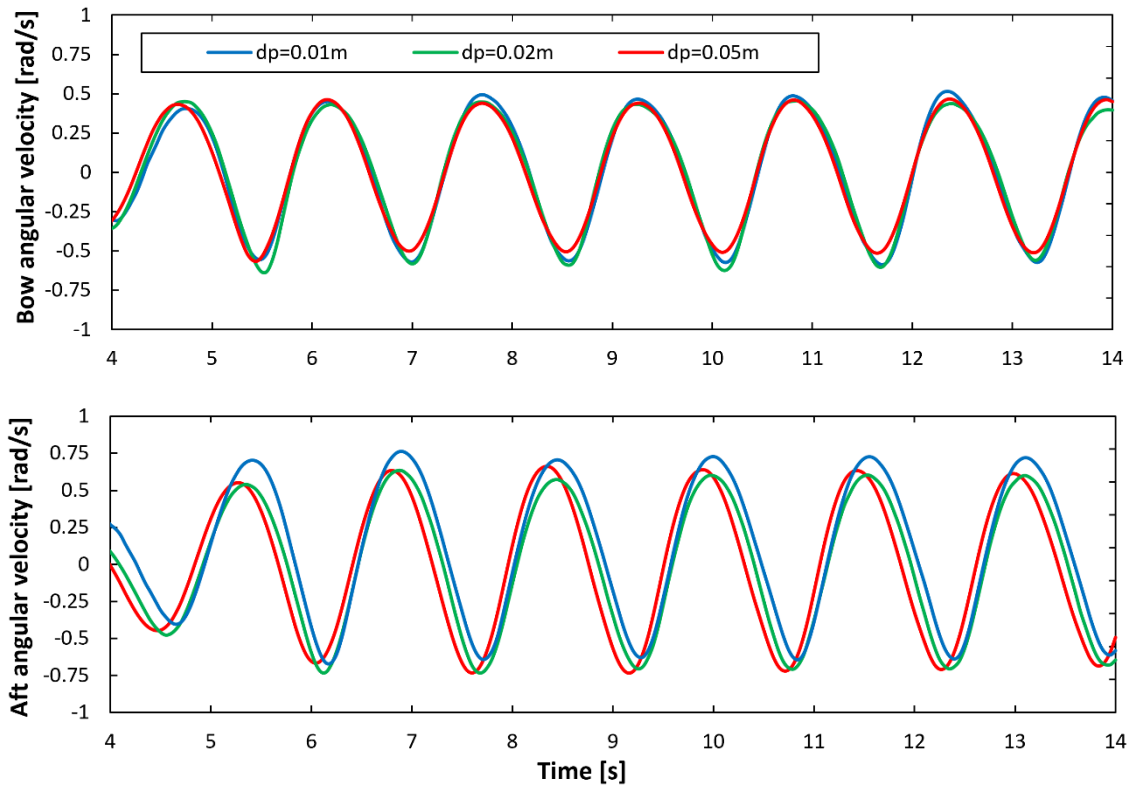


Figure 6.1. Time series of the angular velocity of the flaps for different resolutions.

Considering the flap width of FOSWEC is $D=0.76$ m and using the angular velocity obtained in the simulations with $dp=0.02$ m, we can compute P_w , $P_{a,bow}$, $P_{a,aft}$ and CWR according to the expressions described in previous section. The results are summarised in Table 6.1 where an efficiency of almost 30 % is achieved for the wave condition and PTO configuration of test R5C.

Table 6.1. Power and efficiency results of R5C.

Parameter	Value
P_w	22.537 W
$P_{a,bow}$	4.676 W
$P_{a,aft}$	2.003 W
CWR	29.64 %

6.3 Further numerical study

DualSPHysics is now used to conduct an efficiency study where we have considered different wave conditions and PTO systems:

- i) different wave conditions with six wave periods but same wave height and initial water depth as in the validation case (Table 6.2)
- ii) different PTO configurations using three different damping coefficients (Table 6.3).

Table 6.2. Different wave conditions used in the efficiency study.

H [m]	0.136	0.136	0.136	0.136	0.136	0.136
d [m]	1.360	1.360	1.360	1.360	1.360	1.360
T [s]	1.000	1.125	1.250	1.375	1.563	1.786
L [m]	1.560	1.975	2.440	2.934	3.740	4.720

Table 6.3. Different PTO configurations used in the efficiency study.

	PTO 1	PTO 2	PTO 3
<i>Stiffness</i> [Nm/rad]	0	0	0
<i>Damping (bow)</i> [Nms/rad]	1.762	2.643	3.524
<i>Damping (aft)</i> [Nms/rad]	0.4654	0.6981	0.9308

Therefore, a total of 18 simulations will be executed, where the same resolution of $dp=0.02$ m is employed since it was shown to provide a good balance between accuracy and runtimes during the validation stage.

The wave power and absorbed power by the FOSWEC are represented in Figure 6.2 for the different wave periods and using the three sets of damping coefficients in the PTO system. It can be observed that wave power increases with the wave period while the absorbed power by the device is maximum for wave periods of 1.563 s.

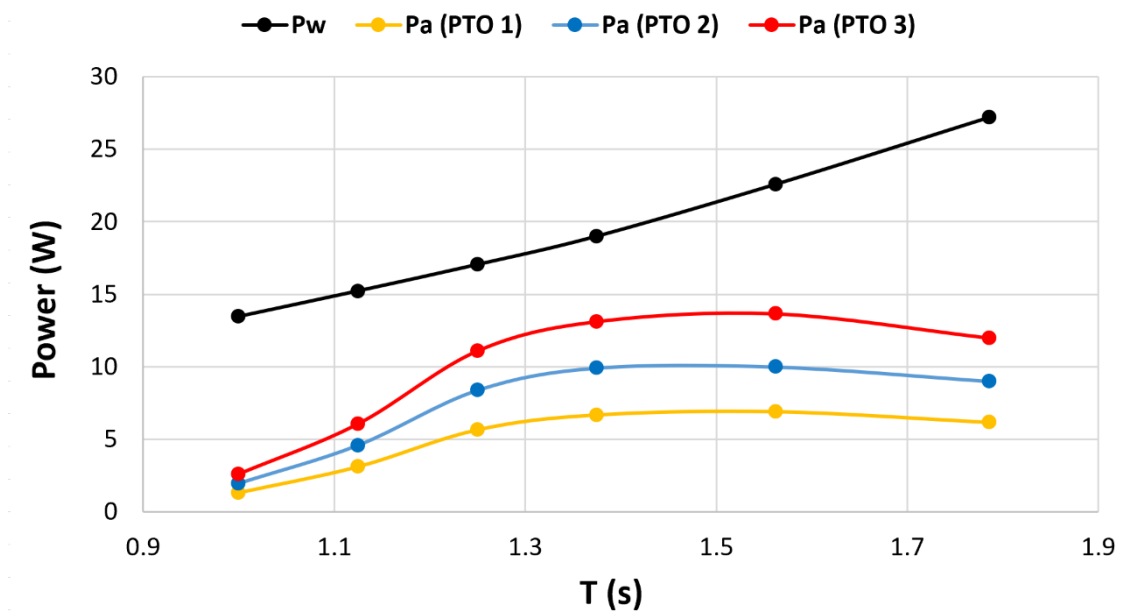


Figure 6.2. Wave power and power absorbed by FOSWEC for different wave periods.

Figure 6.3 shows the efficiency achieved by computing the CWR according to Eq. (19). The efficiency increases with the damping coefficients (Table 6.3). Regarding the wave period, the maximum efficiency is reached for $T=1.375$ s. Analysing the 18 simulations, the maximum efficiency was achieved for the higher damping coefficients in both flaps and for the intermediate wave periods, reaching 70 % of maximum efficiency.

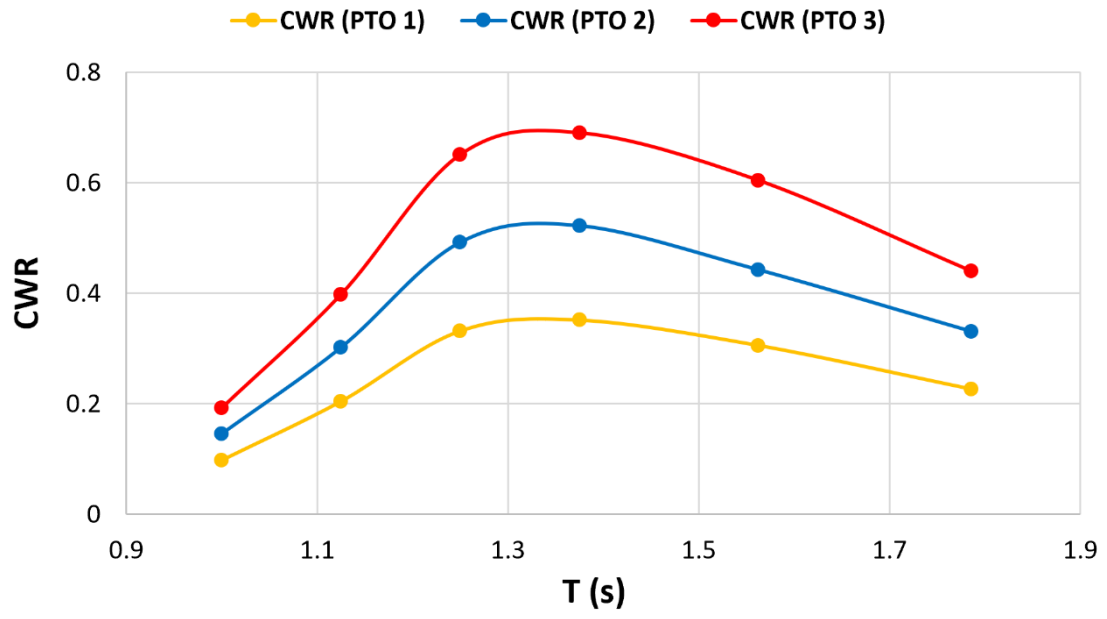


Figure 6.3. Efficiency of FOSWEC as function of wave period and for different PTO systems.

7. Conclusions and future work

This work has shown that the SPH method is a feasible alternative to traditional mesh-based methods when the purpose is to simulate a floating device, like the FOSWEC, under the action of regular waves. It has been proven that SPH methods, and the free software *DualSPHysics* in particular, are able to generate, propagate and absorb waves, and to reproduce the interaction between the FOSWEC and these waves.

In addition, it is also possible to model mechanical restrictions for multibody problems, imposed by the PTO system of FOSWEC, thanks to the coupling of *DualSPHysics* with *Project Chrono* library. On the other hand, the coupling with *MoorDyn* library allows us to reproduce the behaviour of mooring lines.

The *DualSPHysics* software reproduces successfully the experimental case R5C conducted by SANDIA National Laboratories regarding the design of FOSWEC. A good agreement was obtained comparing the experimental and numerical wave elevation, hull motions (heave, surge and pitch) and the flap angles. The numerical tensions of the mooring lines will only agree with the experimental tensions if a very high resolution is used to execute the simulations. However, an intermediate resolution using $dp=0.02$ m, lead to accurate results obtained at reasonable runtimes (7 hours). Obtaining accurate results for a such complex device as the FOSWEC by using only one unique CFD software was very challenging but the results of the validation corroborate the success.

Once the numerical tool was validated, *DualSPHysics* was used to analyse the efficiency of different cases including different wave conditions (different wave periods) and different PTO configurations (different damping values of the PTO). A total number of 18 different tests were executed. The maximum efficiency was achieved for intermediate wave periods and the absorbed power also increases with the damping coefficients of the PTO system. However, those efficiency results have been obtained for these 18 tests, so that continuously increasing damping of the PTO may lead to reach a peak in efficiency, starting from that less efficient configurations will be found for very high values of the PTO damping. In the future, a more complete efficiency study needs to be performed considering much higher PTO damping values than the ones used for this project and other wave conditions. In any case, an efficiency of 70 % was reached for $T=1.375$ s and damping coefficients of 3.524 and 0.9308 Nms/rad in the bow and aft flaps, respectively. This efficiency study evidences that *DualSPHysics* is a very useful tool to help on the design stages of wave energy converters.

Throughout this study only regular waves have been simulated, however it is also possible to reproduce irregular or focused waves, in order to reproduce more realistic ocean and sea conditions. For a future work, it will be of interest not only the study of different wave conditions, but also different configurations of the PTO system, different geometries of the hull and the flaps, studies with different inertia values, novel materials to build the FOSWEC, etc.

It is of special interest, the possibility to run cases under extreme wave conditions, in order to study the survivability of the device, which will help to determine the viability of the FOSWEC to become a real alternative way to obtain energy with zero CO₂ emissions.

This work has been conducted under the supervision of members of the *EPhysLab* group, where one of the main research lines is the development of the wave energy. Note that the research regarding wave energy counts with financial help so that its development can be boosted, as it is considered to be a renewable energy with an important role in the near future.

References

Altomare C., Crespo A.J.C., Domínguez J.M., Gómez-Gesteira M., Suzuki T., Verwaest T. 2015. Applicability of Smoothed Particle Hydrodynamics for estimation of sea wave impact on coastal structures. *Coastal Engineering*, 96, 1-12.

[doi:10.1016/j.coastaleng.2014.11.001](https://doi.org/10.1016/j.coastaleng.2014.11.001).

Altomare C., Domínguez J.M., Crespo A.J.C., González-Cao J., Suzuki T., Gómez-Gesteira M., Troch P. 2017. Long-crested wave generation and absorption for SPH-based DualSPHysics model. *Coastal Engineering*, 127, 37-54.

[doi:10.1016/j.coastaleng.2017.06.004](https://doi.org/10.1016/j.coastaleng.2017.06.004).

Batchelor G K. 1974. *Introduction to fluid dynamics*. Cambridge University Press.

Canelas R.B.C., Crespo A.J.C., Brito M., Domínguez J.M., García-Feal O. 2018. Extending DualSPHysics with a Differential Variational Inequality: modeling fluid-mechanism interaction. *Applied Ocean Research*, 76, 88-97.

[doi:10.1016/j.apor.2018.04.015](https://doi.org/10.1016/j.apor.2018.04.015).

Coe R.G., Bacelli G., Forbush D., Spencer S.J., Dullea K., Bosma B., Lomonaco P. 2020. FOSWEC dynamics and controls test report. Edited by Sandia National Laboratories.

Crespo A.J.C., Gómez-Gesteira M., Dalrymple R.A. 2007. Boundary Conditions Generated by Dynamic Particles in SPH Methods. *CMC: Computers, Materials, & Continua*, 5(3), 173-184.

Crespo A.J.C., Domínguez J.M., Barreiro A., Gómez-Gesteira M. and Rogers B.D. 2011. GPUs, a new tool of acceleration in CFD: Efficiency and reliability on Smoothed Particle Hydrodynamics methods. *PLoS ONE* 6 (6), e20685, [doi:10.1371/journal.pone.0020685](https://doi.org/10.1371/journal.pone.0020685).

Crespo A.J.C., Altomare C., Domínguez J.M., González-Cao J., Gómez-Gesteira M. 2017. Towards simulating floating offshore oscillating water column converters with Smoothed Particle Hydrodynamics. *Coastal Engineering*, 126, 11-26. [doi:10.1016/j.coastaleng.2017.05.001](https://doi.org/10.1016/j.coastaleng.2017.05.001).

Domínguez J.M., Crespo A.J.C., Hall M., Altomare C., Wu M., Stratigaki V., Troch P., Cappiotti L., Gómez-Gesteira M. 2019. SPH simulation of floating structures with moorings. *Coastal Engineering*, 153, 103560. [doi:10.1016/j.coastaleng.2019.103560](https://doi.org/10.1016/j.coastaleng.2019.103560).

Domínguez J.M., Fourtakas G., Altomare C., Canelas R.B., Tafuni A., García-Feal O., Martínez-Estévez I., Mokos A., Vacondio R., Crespo A.J.C., Rogers B.D., Stansby P.K., Gómez-Gesteira M. 2021. DualSPHysics: from fluid dynamics to multiphysics problems. *Computational Particle Mechanics*. [doi:10.1007/s40571-021-00404-2](https://doi.org/10.1007/s40571-021-00404-2).

Eagleson P., Dean R. 1966. Small Amplitude Wave Theory. McGraw-Hill, New York (1966).

ETIPOCEAN, 2020. Strategic Research and Innovation Agenda for Ocean Energy; Ocean Energy Europe: Brussels, Belgium. Available at: <https://www.oceanenergy-europe.eu/wp-content/uploads/2020/05/ETIP-Ocean-SRIA.pdf>.

European Commission, 2020. Regulation Of The European Parliament And Of The Council Establishing The Framework For Achieving Climate Neutrality And Amending Regulation (EU) 2018/1999 (European Climate Law). Available at: <https://eur-lex.europa.eu/legal-content/EN/TXT/?uri=CELEX:52020PC0080>.

Falnes J. 2007. A review of wave-energy extraction. Marine Structures, 20 (4), 185 – 201.

Gotoh H., Khayyer A. 2018. On the state-of-the-art of particle methods for coastal and ocean engineering. Coastal Engineering Journal, 60, 79-103.

IDEA (2011-2020) Plan de Energías Renovables 2011-2020. Instituto para la Diversificación y Ahorro de la Energía.

IPCC (2007) AR4 Climate Change 2007: The Physical Science Basis. The Intergovernmental Panel on Climate Change.

Losada I., Vidal C., Méndez F., Mínguez R., Requejo S., Camus P., Tomás A., Menéndez M., Izaguirre C., Espejo A., González B., Kakeh N., Fernández F., Maza F. 2011. Evaluación del potencial de la energía de las olas. Estudio Técnico PER 2011-2020. Instituto para la Diversificación y Ahorro de la Energía.

Madsen O.S. 1971. On the generation of long waves. J. Geophys. Res. 76: 8672–8683. [doi:10.1029/JC076i036p08672](https://doi.org/10.1029/JC076i036p08672).

Monaghan J. 1992. Smoothed particle hydrodynamics. Annual Review of Astronomy and Astrophysics 30, 543- 574.

Monaghan, J. 1994. Simulating free surface flows with sph. Journal of Computational Physics, 110, 399–4.

Monaghan J., Kos A. 1999. Solitary waves on a Cretan beach. Journal of Waterway, Port, Coastal and Ocean Engineering, 125, 145-154.

Quartier N., Roperio-Giralda P., Domínguez J.M., Stratigaki V., Troch P. 2021. Influence of the Drag Force on the Average Absorbed Power of Heaving Wave Energy Converters Using Smoothed Particle Hydrodynamics. Water, 13(3), 384. [doi:10.3390/w13030384](https://doi.org/10.3390/w13030384).

Ropero-Giralda P., Crespo A.J.C., Tagliafierro B., Altomare C., Domínguez J.M., Gómez-Gesteira M., Viccione G. 2020. Efficiency and survivability analysis of a point-absorber wave energy converter using DualSPHysics. *Renewable Energy*, 162, 1763-1776. [doi:10.1016/j.renene.2020.10.012](https://doi.org/10.1016/j.renene.2020.10.012).

Ropero-Giralda P., Crespo A.J.C., Coe R.G., Tagliafierro B., Domínguez J.M., Bacelli G, Gómez-Gesteira M. 2021. Modelling a heaving point-absorber with a closed-loop control system using the DualSPHysics code. *Energies* 14(3), 760. [doi:10.3390/en14030760](https://doi.org/10.3390/en14030760).

Violeau D. 2012. *Fluid Mechanics and the SPH Method: Theory and Applications*. Oxford University Press.

Wendland H. 1995. Piecewise polynomial, positive definite and compactly supported radial functions of minimal degree. *Advanced in Computational Mathematics* 4, 389-396. [doi:10.1007/BF02123482](https://doi.org/10.1007/BF02123482).

Zhang F., Crespo A.J.C., Altomare C., Domínguez J.M., Marzeddu A., Shang S., Gómez-Gesteira M. 2018. DualSPHysics: a numerical tool to simulate real breakwaters. *Journal of Hydrodynamics*, 30(1), 99-105. [doi:10.1007/s42241-018-0010-0](https://doi.org/10.1007/s42241-018-0010-0).

Appendix

This appendix will include the content of the XML file used to execute the simulations with DualSPHysics.

```
<?xml version="1.0" encoding="UTF-8" ?>
<case app="GenCase v5.0.227 (06-01-2021)"
      date="27-04-2021 11:10:15">
  <casedef>
    <constantsdef>


---


      <mkconfig boundcount="230" fluidcount="9">


---


      <geometry>


---


      <floatings>


---


      <motion>


---


    </casedef>
    <execution>
      <special>


---


        <damping>


---


        <wavepaddles>


---


        <moorings>


---


        <chrono>


---


      </special>
      <parameters>


---


    </execution>
  </case>
```

1. Constant definition (constantsdef & mkconfig)

```
<constantsdef>
  <gravity x="0" y="0" z="-9.81" comment="Gravitational acceleration"
  units_comment="m/s^2" />
  <rhop0 value="1000" comment="Reference density of the fluid"
  units_comment="kg/m^3" />
  <hswl value="0" auto="true" comment="Maximum still water level to calculate
  speedofsound using coefsound" units_comment="metres (m)" />
  <gamma value="7" comment="Polytropic constant for water used in the state
  equation" />
  <speedsystem value="0" auto="true" comment="Maximum system speed (by default
  the dam-break propagation is used)" />
  <coefsound value="20" comment="Coefficient to multiply speedsystem" />
  <speedsound value="0" auto="true" comment="Speed of sound to use in the
  simulation (by default speedofsound=coefsound*speedsystem)" />
  <coefh value="1.5" comment="Coefficient to calculate the smoothing length
  (h=coefh*sqrt(3*dp^2) in 3D)" />
  <cflnumber value="0.2" comment="Coefficient to multiply dt" />
</constantsdef>
<mkconfig boundcount="230" fluidcount="9">
  <mkorientfluid mk="0" orient="Xyz" />
</mkconfig>
```

2. Geometry

```
<geometry>
  <predefinition>
    <newvarcte initialDraft="-0.773" />
    <newvarcte flapZshift="0.26" />
    <newvarcte hingeShift="0.65" />
    <newvarcte wavelength0="3.74" />
    <newvarcte wavelength="4.51" />
    <newvar hingeZ="-0.62" />
  </predefinition>
  <!-- dp = initial particle distance -->
  <definition dp="0.02">
    <pointmin x="-1" y="-1.5" z="-2" />
    <pointmax x="60" y="1.5" z="2" />
  </definition>
  <commands>
  <mainlist>
    <setshapemode>actual | dp | bound</setshapemode>
    <setdrawmode mode="full" />
    <!-- PISTON -->
    <setmkbound mk="10" />
    <drawbox>
      <boxfill>solid</boxfill>
      <point x="#0-5*Dp" y="-2" z="-1.36" />
      <size x="#5*Dp" y="4" z="2" />
    </drawbox>
    <shapeout file="piston" reset="true" />
    <!-- BOTTOM+SLOPE -->
    <setmkbound mk="0" />
    <setfrdrawmode auto="true" />
    <drawextrude closed="false">
    <extrude x="0" y="4" z="0" />
      <point x="-0.5" y="-2" z="-1.36" />
      <point x="6.7" y="-2" z="-1.36" />
      <point x="11.2" y="-2" z="0.35" />
      <layers vdp="0*,-1,-2,-3" />
    </drawextrude>
    <setfrdrawmode auto="false" />
    <shapeout file="tank" reset="true" />
    <setdrawmode mode="full" />

    <!-- FOSWEC -->
    <setmkbound mk="50" />
    <drawfilestl file="body.stl">
      <drawscale x="1" y="1" z="1" />
      <drawmove x="#wavelength" y="0" z="#initialDraft" />
      <drawrotate angx="0" angy="0" angz="0" />
    </drawfilestl>
    <!-- Filling parts of the hull -->
    <fillbox x="4.5" y="0" z="-0.75">
      <modefill>void</modefill>
      <point x="3.5" y="-2" z="-1.5" />
      <size x="5" y="4" z="2" />
    </fillbox>
    <fillbox x="3.85" y="0.7" z="-0.7">
      <modefill>void</modefill>
      <point x="3.5" y="-2" z="-1.5" />
      <size x="5" y="4" z="2" />
    </fillbox>
    <fillbox x="3.85" y="-0.7" z="-0.7">
      <modefill>void</modefill>
      <point x="3.5" y="-2" z="-1.5" />
      <size x="5" y="4" z="2" />
    </fillbox>
    <fillbox x="5.2" y="0.7" z="-0.7">
      <modefill>void</modefill>
      <point x="3.5" y="-2" z="-1.5" />
      <size x="5" y="4" z="2" />
    </fillbox>
    <fillbox x="5.2" y="-0.7" z="-0.7">
```

```

        <modefill>void</modefill>
        <point x="3.5" y="-2" z="-1.5" />
        <size x="5" y="4" z="2" />
    </fillbox>
    <fillbox x="5.2" y="-0.7" z="0.2">
    <modefill>void</modefill>
        <point x="3.5" y="-2" z="-1.5" />
        <size x="5" y="4" z="2" />
    </fillbox>
    <fillbox x="3.87" y="0.47" z="-0.75">
        <modefill>void</modefill>
        <point x="3.5" y="-2" z="-1.5" />
        <size x="5" y="4" z="2" />
    </fillbox>
    <fillbox x="3.87" y="-0.47" z="-0.75">
        <modefill>void</modefill>
        <point x="3.5" y="-2" z="-1.5" />
        <size x="5" y="4" z="2" />
    </fillbox>
    <fillbox x="5.17" y="0.47" z="-0.75">
        <modefill>void</modefill>
        <point x="3.5" y="-2" z="-1.5" />
        <size x="5" y="4" z="2" />
    </fillbox>
    <fillbox x="5.17" y="-0.47" z="-0.75">
        <modefill>void</modefill>
        <point x="3.5" y="-2" z="-1.5" />
        <size x="5" y="4" z="2" />
    </fillbox>
    <fillbox x="5.17" y="-0.47" z="2">
        <modefill>void</modefill>
        <point x="3.5" y="-2" z="-1.5" />
        <size x="5" y="4" z="2" />
    </fillbox>
    <shapeout file="body" reset="true" />
    <!-- FLAP BOW -->
    <setmkbound mk="101" />
    <drawfilestl file="flap.stl" autofill="true">
        <drawscale x="1" y="1" z="1" />
        <drawmove x="#wavelength-hingeShift" y="0"
            z="#initialDraft+flapZshift" />
        <drawrotate angx="0" angy="0" angz="0" />
    </drawfilestl>
    <!-- FLAP AFT -->
    <setmkbound mk="102" />
    <drawfilestl file="flap.stl" autofill="true">
        <drawscale x="1" y="1" z="1" />
        <drawmove x="#wavelength+hingeShift" y="0"
            z="#initialDraft+flapZshift" />
        <drawrotate angx="0" angy="0" angz="0" />
    </drawfilestl>
    <shapeout file="flap" reset="true" />
    <!-- FLUID -->
    <setmkfluid mk="0" />
    <fillbox x="0.5" y="0" z="-0.05">
        <modefill>void</modefill>
        <point x="-1" y="-2" z="-1.5" />
        <size x="40" y="4" z="1.52" />
    </fillbox>
    <shapeout file="" reset="true" />
</mainlist>
</commands>
</geometry>

```

3. Rigid bodies definition (floatings)

```
<floatings>
  <floating mkbound="50">
    <massbody value="276" />
    <center x="#wavelength" y="0" z="-0.7296" />
    <inertiafull>
      <values v11="43.4615" v12="-4.3483" v13="0.0074" />
      <values v21="-4.3483" v22="49.3573" v23="-0.0074" />
      <values v31="0.0074" v32="-0.0074" v33="77.7506" />
    </inertiafull>
    <translationDOF x="1" y="0" z="1" comment="Use 0 for translation
restriction in the acceleration calculation (default=(1,1,1))" />
    <rotationDOF x="1" y="1" z="1" comment="Use 0 for rotation restriction
in the acceleration calculation (default=(1,1,1))" />
  </floating>
  <floating mkbound="101">
    <massbody value="6" />
    <center x="#wavelength-hingeShift" y="0" z="#hingeZ+0.4663" />
  </floating>
  <floating mkbound="102">
    <massbody value="6" />
    <center x="#wavelength+hingeShift" y="0" z="#hingeZ+0.4663" />
  </floating>
</floatings>
```

4. Motion

```
<motion>
  <objreal ref="10">
    <begin mov="1" start="0" />
      <mvnull id="1" />
    </objreal>
</motion>
```

5. Damping zone

```
<damping>
  <dampingzone>
    <limitmin x="6.7" y="0" z="0" />
    <limitmax x="11" y="0" z="0" />
    <overlimit value="1" />
    <redumax value="10" />
  </dampingzone>
</damping>
```

6. Automatic wave generator (regular waves)

```
<wavepaddles>
  <piston>
    <mkbound value="10" comment="Mk-Bound of selected particles" />
    <waveorder value="2" comment="Order wave generation 1:1st order, 2:2nd
order (def=1)" />
    <start value="0" comment="Start time (default=0)" />
    <duration value="0" comment="Movement duration, Zero is the end of
simulation (def=0)" />
    <depth value="1.36" comment="Fluid depth (def=0)" />
    <pistondir x="1" y="0" z="0" comment="Movement direction
(def=(1,0,0))" />
    <waveheight value="0.136" comment="Wave height" />
    <waveperiod value="1.5625" comment="Wave period" />
    <gainstroke value="1.0" comment="Gain factor to amplify/reduce the
paddle stroke (default=1)" />
    <phase value="0" comment="Initial wave phase in function of PI (def=0)"
/>
    <ramp value="1" comment="Periods of ramp (def=0)" />
    <savemotion periods="20" periodsteps="50" xpos="3.74" zpos="-0.1"
comment="Saves motion data. xpos and zpos are optional. zpos=-depth of
the measuring point" />
  </piston>
</wavepaddles>
```

7. Mooring configuration (MoorDyn library)

```
<moorings>
  <savevtk_moorings value="true" comment="Saves vtk with moorings
(default=true)" />
  <savecsv_points value="true" comment="Saves csv with link points
(default=true)" />
  <savevtk_points value="false" comment="Saves vtk with link
points (default=false)" />
  <mooredfloatings>
    <floating mkbound="50" comment="Mkbound of the Floating body the
mooring is linked to" />
  </mooredfloatings>
  <moordyn comment="MoorDyn configuration">%Loads the next configuration
  <solverOptions>
    <waterDepth value="1.36" comment="Water depth" units_comment="m" />
    <freesurface value="0" comment="Z position of the water free
surface. (default=0)" />
    <kBot value="3.0e6" comment="Bottom stiffness constant. (default=3.0e6)"
units_comment="Pa/m" />
    <cBot value="3.0e5" comment="Bottom damping constant. (default=3.0e5)"
units_comment="Pa*s/m" />
    <dtM value="0.001" comment="Desired mooring model time step. (default=0.0001)"
/>
    <waveKin value="0" comment="Wave kinematics flag ( 0: neglect [the only option
currently supported] ). (default=0)" />
    <writeUnits value="yes" comment="Write units line. value=[yes|no].
(default=yes)" />
    <frictionCoefficient value="0" comment="General bottom friction coefficient,
as a start. (default=0.0)" />
    <fricDamp value="200" comment="Damping coefficient used to model the friction
with speeds near zero. (default=200.0)" />
    <statDynFricScale value="1.0" comment="Ratio between static and dynamic
friction (mu_static/mu_dynamic). (default=1.0)" />
    <dtIC value="1.0" comment="Period to analyse convergence of dynamic relaxation
for initial conditions. (default=1.0)" units_comment="s" />
    <cdScaleIC value="2" comment="Factor to scale drag coefficients during dynamic
relaxation for initial conditions. (default=5)" />
    <threshIC value="0.001" comment="Convergence threshold for for initial
conditions. (default=0.001)" />
    <tmaxIC value="1" comment="Maximum time for initial conditions without
convergence. (default=0)" units_comment="s" />
  </solverOptions>
```

```

<bodies>
  <body ref="50" comment="Floating driven structure to attach mooring
lines." />
</bodies>
<lines>
  <linedefault comment="Shared properties for each line.">
    <ea value="80000" units_comment="N" />
    <diameter value="0.0035" comment="Volume-equivalent diameter of
the line." units_comment="m" />
    <massDenInAir value="0.07" comment="Mass per unit length of the
line." units_comment="kg/m" />
    <ba value="-0.8" comment="Line internal damping (BA/-zeta).
(default=-0.8)" units_comment="Ns" />
    <can value="1.0" comment="Transverse added mass coefficient
(with respect to line displacement). (default=1.0)" />
    <cat value="0.0" comment="Tangential added mass coefficient
(with respect to line displacement). (default=0.0)" />
    <cdn value="1.6" comment="Transverse drag coefficient (with
respect to frontal area, d*1). (default=1.6)" />
    <cdt value="0.05" comment="Tangential drag coefficient (with
respect to surface area, n*d*1). (default=0.05)" />
    <outputFlags value="t" comment="Node output
properties. (default=-) [-:None|p:Positions|v:Velocities|U:Wave
Velocities|t:Tension|D:Hydrodynamic Drag Force|c:Internal
Damping|s:Strain of each segment|d: rate of strain of each
segment]" />
  </linedefault>
  <line>%line 0
    <vesselconnection bodyref="50" x="3.86" y="0.70" z="-1.02" />
    <fixconnection x="3.86" y="0.70" z="-1.36" />
    <length value="0.341" comment="(m)" />
    <segments value="20" />
  </line>
  <line>%line 1
    <vesselconnection bodyref="50" x="3.86" y="-0.70" z="-1.02" />
    <fixconnection x="3.86" y="-0.70" z="-1.36" />
    <length value="0.341" comment="(m)" />
    <segments value="20" />
  </line>
  <line>%line 2
    <vesselconnection bodyref="50" x="5.16" y="0.70" z="-1.02" />
    <fixconnection x="5.16" y="0.70" z="-1.36" />
    <length value="0.341" comment="(m)" />
    <segments value="20" />
  </line>
  <line>%line 3
    <vesselconnection bodyref="50" x="5.16" y="-0.70" z="-1.02" />
    <fixconnection x="5.16" y="-0.70" z="-1.36" />
    <length value="0.341" comment="(m)" />
    <segments value="20" />
  </line>
</lines>
  <output comment="Output data properties for each line.">
    <time startTime="0" endTime="0" dtOut="0.01" comment="Default
[startTime= 0; endTime= 0; dtOut=0.01]" />
    <tension type="all" comment="Stores tensions at the connections.
type=[fixed|vessel|all]. (default: type=all)" />
    <position type="all" comment="Stores positions at the connections.
type=[fixed|vessel|all]. (default: type=all)" />
  </output>
</moordyn>
</moorings>

```

8. Hinge configuration (Project Chrono library)

```
<chrono>
  <savedata value="0.01" comment="Saves CSV with data exchange for each
  time interval (0=all steps)" />
  <schemescale value="1" comment="Scale used to create the initial scheme of
  Chrono objects (default=1)" />
  <collision activate="false">
    <distancedp value="0.1" comment="Allowed collision overlap according
    Dp (default=0.5)" />
    <contactmethod value="0" comment="Contact method type. 0:NSC (Non
    Smooth Contacts), 1:SMC (SMooth Contacts). (default=0)" />
    <ompthreads value="1" comment="Number of threads by host for parallel
    execution. 0:Muli Core, 1:Single Core (default=1)" />
  </collision>
  <bodyfloating id="body" mkbound="50" modelfile="AutoActual" />
  <bodyfloating id="flapBow" mkbound="101" modelfile="AutoActual" />
  <bodyfloating id="flapAft" mkbound="102" modelfile="AutoActual" />
  <link_hinge idbody1="body" idbody2="flapBow">
    <rotpoint x="#wavelength-hingeShift" y="0" z="#hingeZ"
    comment="Point for rotation" />
    <rotvector x="0" y="1" z="0" comment="Vector direction for
    rotation" />
    <stiffness value="-3.561" comment="Torsional stiffness [Nm/rad]" />
    <damping value="1.762" comment="Torsional damping [Nms/rad]" />
  </link_hinge>
  <link_hinge idbody1="body" idbody2="flapAft">
    <rotpoint x="#wavelength+hingeShift" y="0" z="#hingeZ"
    comment="Point for rotation" />
    <rotvector x="0" y="1" z="0" comment="Vector direction for
    rotation" />
    <stiffness value="-2.800" comment="Torsional stiffness [Nm/rad]" />
    <damping value="0.4654" comment="Torsional damping [Nms/rad]" />
  </link_hinge>
</chrono>
```

9. SPH Parameters

```
<parameters>
  <parameter key="SavePosDouble" value="1" comment="Saves particle position
  using double precision (default=0)" />
  <parameter key="StepAlgorithm" value="2" comment="Step Algorithm 1:Verlet,
  2:Symplectic (default=1)" />
  <parameter key="VerletSteps" value="40" comment="Verlet only: Number of steps
  to apply Euler timestepping (default=40)" />
  <parameter key="Kernel" value="2" comment="Interaction Kernel 1:Cubic Spline,
  2:Wendland (default=2)" />
  <parameter key="ViscoTreatment" value="1" comment="Viscosity formulation
  1:Artificial, 2:Laminar+SPS (default=1)" />
  <parameter key="Visco" value="0.01" comment="Viscosity value" />
  <parameter key="ViscoBoundFactor" value="0" comment="Multiply viscosity value
  with boundary (default=1)" />
  <parameter key="DensityDT" value="2" comment="Density Diffusion Term 0:None,
  1:Molteni, 2:Fourtakas, 3:Fourtakas(full) (default=0)" />
  <parameter key="DensityDTvalue" value="0.0" comment="DDT value (default=0.1)"
  />
  <parameter key="Shifting" value="0" comment="Shifting mode 0:None,
  1:Ignore bound, 2:Ignore fixed, 3:Full (default=0)" />
  <parameter key="ShiftCoef" value="-2" comment="Coefficient for shifting
  computation (default=-2)" />
  <parameter key="ShiftTFS" value="0" comment="Threshold to detect free surface.
  Typically 1.5 for 2D and 2.75 for 3D (default=0)" />
  <parameter key="RigidAlgorithm" value="3" comment="Rigid Algorithm
  0:collision-free, 1:SPH, 2:DEM, 3:Chrono (default=1)" />
  <parameter key="FtPause" value="0.0" comment="Time to freeze the floatings at
  simulation start (warmup) (default=0)" units_comment="seconds" />
  <parameter key="CoefDtMin" value="0.05" comment="Coefficient to calculate
  minimum time step dtmin=coefdtmin*h/speedsound (default=0.05)" />
</parameters>
```

```

<parameter key="DtIni" value="0" comment="Initial time step. Use 0 to default
use (default=h/speedsound)" units_comment="seconds" />
<parameter key="DtMin" value="0" comment="Minimum time step. Use 0 to default
use (default=coefdtmin*h/speedsound)" units_comment="seconds" />
<parameter key="DtFixed" value="0" comment="Fixed Dt value. Use 0 to disable
(default=disabled)" units_comment="seconds" />
<parameter key="DtFixedFile" value="NONE" comment="Dt values are loaded from
file. Use NONE to disable (default=disabled)" units_comment="milliseconds
(ms)" />
<parameter key="DtAllParticles" value="0" comment="Velocity of particles used
to calculate DT. 1:All, 0:Only fluid/floating (default=0)" />
<parameter key="TimeMax" value="14" comment="Time of simulation"
units_comment="seconds" />
<parameter key="TimeOut" value="0.05" comment="Time out data"
units_comment="seconds" />
<parameter key="PartsOutMax" value="1" comment="%/100 of fluid particles
allowed to be excluded from domain (default=1)" units_comment="decimal" />
<parameter key="RhopOutMin" value="700" comment="Minimum rhop valid
(default=700)" units_comment="kg/m^3" />
<parameter key="RhopOutMax" value="1300" comment="Maximum rhop valid
(default=1300)" units_comment="kg/m^3" />
<parameter key="YPeriodicIncZ" value="0.0" comment="Increase of Z with
periodic BC" units_comment="metres (m)" />
<simulationdomain comment="Defines domain of simulation (default=Uses minimun
and maximum position of the generated particles)">
  <posmin x="default" y="default" z="default" />
  <posmax x="default" y="default" z="default" />
</simulationdomain>
</parameters>

```